Wood Nanotechnologies for Transparency, Fire Retardancy and Liquid Separation

Qiliang Fu

Doctoral Thesis
Stockholm, Sweden, 2018

Department of Fiber and Polymer Technology
School of Engineering Sciences in Chemistry, Biotechnology and Health
KTH Royal Institute of Technology

Principal supervisor
Professor Lars A. Berglund

Co-supervisor
Professor Qi Zhou

ISBN 978-91-7729-671-3
TRITA-CBH-FOU-2018:1
ISSN 1654-1081

AKADEMISK AVHANDLING

Som med tillstånd av Kungliga Tekniska Högskolan i Stockholm framlägges till offentlig granskning för avläggande av teknologie doktorsexamen fredagen den 07 mars 2018, kl. 10.00 i sal F3, Lindstedtsvägen 26, KTH, Stockholm. Avhandlingen försvaras på engelska.
Opponent: Professor Hiroyuki Yano, Kyoto University, Japan.

You never fail until you stop trying.

---Albert Einstein

ABSTRACT

In this thesis, wood nanotechnologies for transparent, fire-retardant and hydrophobic/lipophilic wood have been developed. There are two main parts; wood template preparation/processing concepts and materials design using these templates.

In the wood template processing part, highly porous nanostructured wood templates are prepared. Relationships between processes and material structures are studied. Three chemical treatment methods are used. Lignin and/or chromophores are removed from cell wall, so that nanoscale pores are formed in the cell wall. For preparation of transparent wood, a lignin-retaining method improves physical properties of the template. The pore structures are characterized by scanning electron microscopy and gas adsorption measurement of specific surface area. The compositions of the templates are characterized. Compared with native wood, these templates have nanoscale porosity which provides opportunity for new types of wood modification.

In the materials design part, wood nanotechnologies are used for transparent wood as well as for hydrophobic/lipophilic and fire-retardant wood. Two main strategies are used: i) nanoparticles are embedded inside the cell wall; ii) polymers are impregnated in lumen space, and sometimes also inside the cell wall. The transparent wood is prepared by MMA monomer/oligomer impregnation of lumen space. MMA has similar refractive index to the delignified template, so that scattering is reduced and transparent wood with favorable optical and mechanical properties is obtained. The structure and functional properties are studied. Laminated transparent plywood is designed to modify mechanical properties. Transparent wood and transparent plywood are demonstrated in applications combining loading-bearing properties with optical performance such as luminescent properties.

The highly porous wood template cell walls are also impregnated with colloidal montmorillonite clay or epoxy/amine solutions to modify the cell wall and form nanostructured biocomposites. The structure and properties of the two materials are investigated; wood/clay hybrids for flame-retardancy and wood/epoxy biocomposites for oil/water separation.

SAMMANFATTNING

Nanoteknik för trä har utvecklats för transparent trä, brandbeständigt trä och trä för vätskeseparation. Avhandlingen innehåller dels studier av nanoporösa trätemplat, deras framställning och struktur, och dels materialdesign där dessa templat är startmaterial för modifierat trä.

Porösa träbaserade templat har framställts, med porositet på olika skalor (10 μm och 10 nm). Samband mellan process och materialstruktur har undersökts. Tre kemiska metoder har utnyttjats. Lignin och/eller kromoforer avlägsnas från cellväggen så att porer på nanoskala bildas. För transparent trä utvecklas en metod där ligninet endast delvis avlägsnas, eftersom det leder till bättre fysikaliska och mekaniska egenskaper hos substratet. Porstrukturen karakteriseras med svepeletronmikroskopi och gasasdsorption. Kemisk sammansättning karakteriseras. Jämfört med nativ ved så har dessa templat ökad porositet på nanoskala som ger nya möjligheter till vedmodifiering.

Templaten används för transparent trä, liksom för hydrofobt/hydrofilt trä liksom brandhärdigt trä. Oorganiska nanopartiklar modifierar cellväggen i brandhärdigt trä, medan övriga metoder betonar polymerimpregnering, dels i lumen men också i själva cellväggen. Transparent trä framställs genom att lumen fylls med MMA-monomer och polymeriseras. PMMA har ett brytningsindex som ligger nära cellulosa. Ljusspridning minskar och materialet får goda optiska och mekaniska egenskaper. Struktur och funktionella egenskaper studeras. Transparent plywood framställs för att modifiera optiska och mekaniska egenskaper.

Vedtemplat impregneras också med nanopartiklar av lera (montmorillonit), eller epoxy/aminblandningar. Dessa nanokompositer har modifierad cellvägg och är en typ av biokompositer. Struktur-egenskapsrelationer undersöks, dels för organiska/oorganiska hybrider med förbättrade brandegenskaper och dels för tillämpningar där olja och vatten kan separeras.

LIST OF PAPERS

This thesis is a summary of the following five appended papers:
*(co-first author)

I. **Optically transparent wood from a nanoporous cellulosic template: combining functional and structural performance**
Yuanyuan Li*, Qiliang Fu*, Shun Yu, Min Yan, and Lars A. Berglund
Biomacromolecules, 17(4), 1358-1364, 2016

II. **Lignin-retaining transparent wood**
Yuanyuan Li, Qiliang Fu, Ramiro Rojas, Min Yan, Martin Lawoko, and Lars A. Berglund
ChemSusChem, 10(17), 3445-3451, 2017

III. **Transparent plywood as a load-bearing and luminescent biocomposite**
Qiliang Fu, Min Yan, Erik Jungstedt, Xuan Yang, Yuanyuan Li, and Lars A. Berglund
Submitted manuscript

IV. **Nanostructured wood hybrids for fire retardancy prepared by clay impregnation into the cell wall**
Qiliang Fu, Lilian Medina, Yuanyuan Li, Federico Carosio, Alireza Hajian, and Lars A. Berglund
ACS Applied Materials & Interfaces, 9(41), 36154-36163, 2017

V. **Wood nanotechnology for strong, mesoporous, and hydrophobic biocomposites for selective separation of oil/water mixtures**
Qiliang Fu, Farhan Ansari, Qi Zhou, and Lars A. Berglund
ACS Nano, DOI: 10.1021/acsnano.8b00005, 2018

The author's contributions to the appended papers are as follows:

I. Co-first author: Participated in all planning; designed and performed most of the experiments; wrote part of the manuscript.

II. Second author: Participated in part of planning; performed part of the experiments and analyzed part of data.

III. First author: Participated in all planning; designed and performed most of the experimental work; and wrote most of the manuscript.

IV. First author: Participated in all planning; designed and performed most of the experimental work (except cone calorimetry test); and wrote most of the manuscript.

V. First author: Participated in all planning; designed and performed all the experiments; wrote most of the manuscript.

Other publications not included in the thesis

VI. Transparent wood for functional and structural applications
Yuanyuan Li*, Qiliang Fu*, Xuan Yang*, and Lars A. Berglund
Phil. Trans. R. Soc. A, 376 (2112), 20170182, 2018

VII. Towards centimeter thick transparent wood through interface manipulation mination
Yuanyuan Li, Xuan Yang, Qiliang Fu, Ramiro Rojas, Min Yan, Lars Berglund
Journal of Materials Chemistry A, 6(3), 1094-1101, 2018

VIII. Recyclable and superelastic aerogels based on carbon nanotubes and carboxymethyl cellulose
Alireza Hajian, Qiliang Fu, and Lars A. Berglund
Composites Science and Technology, DOI: 10.1016/j.compscitech.2018.01.002, 2018

Abbreviations and Symbols

CNF	Cellulose nanofiber or cellulose nanofibril
L	Longitudinal direction
T	Transverse direction
H	Horizontal direction
V	Vertical direction
TEM	Transmission electron microscopy
1D, 2D, 3D	One, two and three dimensional
l×w×t	Length, width and thickness
TW	Transparent wood
PMMA	Poly(methyl methacrylate)
AIBN	2,2′-azobis iso butyronitrile
MTM	Montmorillonite
DGEBA	Diglycidyl ether of bisphenol A
PEA	Polyether amine
PAA	Peracetic acid
QD	Quantum dot
DTPA	Diethylenetriamine pentaacetic acid
TPW	Transparent plywood
FE-SEM	Field-emission scanning electron microscopy
BET	Brunauer–Emmett–Teller
SSA	Specific surface area
EDX	Energy-dispersive X-ray spectroscopy
TG	Thermogravimetric analysis
TTI	Time to ignition
pKHRR	Peak of heat release rate
THR	Total heat release
SPR	Smoke production rate
TSR	Total smoke release
SAXS	Small angle X-ray scattering
FTIR	Fourier-transform infrared spectroscopy
UV	Ultraviolet
MC	Moisture content
BJH	Barrett-Joyner-Halenda
RH	Relative humidity
AVE	Advanced video extensometer
V_f	Cellulose volume fraction
cp-	Cross-ply

qi-	Quasi-isotropic
E	Young's modulus
E^a	Estimated Young's modulus
σ	Ultimate strength
σ_y	Yield strength
ε	Strain
wt	Weight
vol	Volume

CONTENTS

1. Introduction

Wood is a biological structural material of large importance for the development of human society. As the starting material for chemicals, wood is used to prepare wood pulp fiber, tar, and charcoal. Wood is largely applied as a construction material in the building sector due to high strength-to-weight ratio, eco-friendly characteristics, biodegradability, and aesthetic characteristics. During processing and service, wood suffers problems from fungi, UV-radiation, fire, moisture-related warping, cracking, and dimensional instability. Addressing these problems was the original purpose of wood modification.

Tarkow et al. worked on acetylation of wood with colleagues in 1946.[1] The term "chemical modification of wood" started to be used at this time. Chemical modification of wood is usually defined as involving covalent bonds between chemical groups in the modification agent and some reactive part of the cell wall components.[2] To achieve this, wood cell wall swelling is desirable. However, swelling and bulking of cell walls is limited by low porosity of the cell wall, requiring for miscibility between the modification agent and the cell wall, and chemical solution permeation. If we could increase the porosity of cell wall and change the chemistry of wood cell wall, we could make a new bioarchitecture of wood-based composites with novel functionalities other than what nature gives. This ambition goes further than to just reduce problems with moisture sensitivity, but also looks for new wood material functionalities. In this thesis, "wood nanotechnology" is applied to design functional materials based on wood, using its hierarchical structure to achieve specific property combinations.

1.1 Structure of wood

1.1.1 Macro- and micro- structure of wood

Wood tissue is a hierarchically designed material that consists of complex organizations providing high strength and lightweight from macro- to nano-scales (Figure 1.1).[3] Two main functions are fulfilled by the wood tissue - (i) provide the necessary mechanical support and (ii) transport water and nutrients through the tree.[4] To fulfill this, the cellular material is arranged at different length scales, where fibrous tracheid cells in softwoods can be approximated as hexagonal tubes. The lumen and vessels conduct the majority of the fluids up the tree, while ray cells and pits transport the liquid and nutrients in the radial direction.

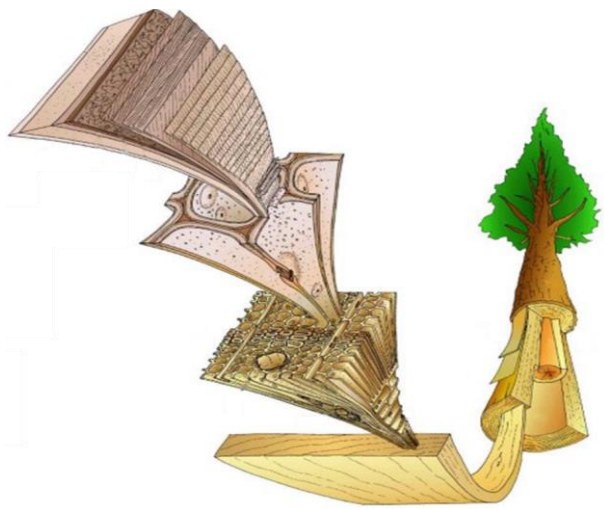

Figure 1.1 Sketch showing the hierarchical structure of wood. From the macroscopic scale of a tree to the microscopic cell wall. (Artwork from Dr. Harrington, University of Canterbury, New Zealand).[3]

Wood species are divided into two categories – softwood and hardwood. The xylem tissue is composed of two different types of cells and we define two directions, the longitudinal (L) and transverse (T) directions (Figure 1.2a,c). The T direction is the radial direction in the figure. The wood substrate in softwood is composed of tracheids (85-95%) and ray cells (2-12%) (Table 1.1).

Softwoods and hardwoods have different cellular structure, see in Figure 1.2. The softwood tracheid gives mechanical strength and provides for water transport through lumen spaces with large cavities (Figure 1.2b). The highly elongated cells which make up the bulk of hardwood are called fibers (37-70%) (Table 1.1). Ray cells (10-32%) are in radial direction (Figure 1.2b,d).

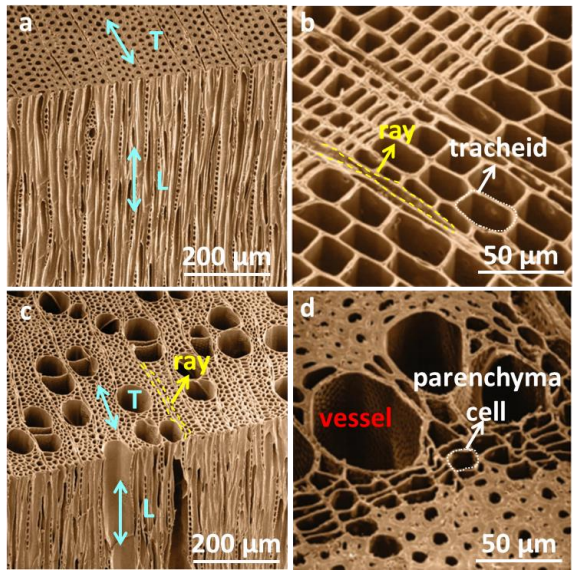

Figure 1.2 The morphology of the softwood and hardwood. (a) The 3D cell wall structure of the softwood European larch (*Larix decidua*) and (b) the border between early wood and late wood in larch. (c) The 3D cell wall structure of the hardwood poplar (*Populus sp.)* and (d) the border between early wood and late wood in poplar.[4] (Copyright © 2006, Springer)

Softwood has a comparatively simple and uniform structure compared with hardwood. Hardwoods have fewer fiber-like cells than softwoods and these are generally shorter in length (Table 1.1). Hardwood vessels provide mostly uninterrupted channels in earlywood (Figure 1.2d and Table 1.1). This is of great importance for liquid conduction. Vessels are mainly thin-walled and are rather short (0.2-1.3 mm) and wide (20-500 µm) elements, which are stacked to form at long tube. The long tubes are more or less completely connected to each other end to end.

Table 1.1 Volume fractions and dimensions of wood cells.[5]

	Softwoods		Hardwoods		
	Tracheid	Ray cells	Fiber	Vessel	Ray cells
Volume fraction (%)	85-95	5-12	37-70	6-55	10-32
Axial dimension (mm)	2.5-7.0		0.6-2.3	0.2-1.3	
Tangential dimension (μm)	25-80		10-30	20-500	
Radial dimension (μm)	17-60		10-30	20-350	
cell-wall thickness (μm)	2-7		1-11		

1.1.2 Ultrastructure of cell wall

The 2D honeycomb structure of wood provides mechanical support for the tree (Figure 1.3a).[3] The cell wall (thickness is 1-11 μm) consists of primary wall, secondary wall and middle lamella (Figure 1.3b). The secondary cell wall dominates, making up roughly 80% of the cell wall, and is based on three layers, out (S1), middle (S2) and inner (S3) layers (Figure 1.3c). The thickest layer of S2 possesses around 85 vol% of the whole secondary wall. In each layer, the solid cell wall is mainly composed of cellulose, hemicellulose, and lignin (Figure 1.3d). Cellulose nanofibrils (~45 wt%) are fibrous elements. They are reinforcing elements in the cell wall, embedded in amorphous polymer matrix of lignin (~25 wt%) and hemicelluloses (~30 wt%). The matrix is a molecular scale mixture of hemicellulose and lignin. In native wood, cell wall is hydrated and contains around 30% of water. Between adjacent cells, cell wall corners are formed, and constitute a lignin-rich region.

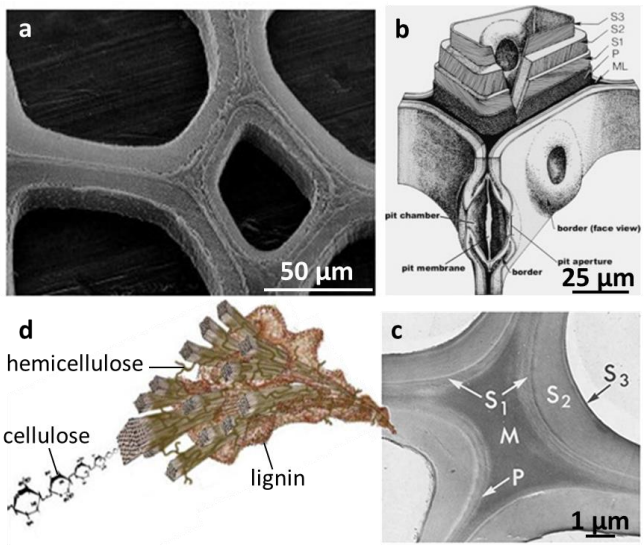

Figure 1.3 The ultrastructure of the cell wall from micron-scale to molecular scale. (a) the cell wall.[3] (From Dr. Harrington, University of Canterbury, New Zealand) (b) A cut-away drawing of the cell wall including the structural details of cell wall organization and a bordered pit.[6] (Copyright © 2005 by CRC Press) (c) TEM image of cell wall showing the middle lamella, cell wall corner, primary cell wall (P), and the secondary wall (S1, S2 and S3 layers).[7] (Copyright © 1993 Academic Press Inc.) (d) the cell wall components at the molecular scale.[3] (From Dr. Harrington, University of Canterbury, New Zealand)

The porosity in the wood tissue is very important. Because of the nature of technological processes, such as drying, impregnation and steaming, small-scale porosity in the cell wall is influenced by these treatements.[8,9] The pores in the wood are divided into three categories, viz. macropores (> 50 nm), mesopores (between 2 nm and 50 nm) and micropores (< 2 nm). The majority of the pores in wood is tracheid lumen (softwood) or vessel (hardwood) and is in the diameter range of 10-500 µm. When a liquid solution enters wood tissue for modification purpose, the liquid, in the initial step, flows from larger pores to the interior of wood tissue through vessels, tracheids and rays.[10] Additional material transport between cells is proposed through pits and the network of

middle lamella and cell wall corner regions. The pores in the cell wall are sub-micropores or even molecular scale. This means great difficulties for meso-scale particles and large molecular weight incompatible polymers to enter inside the cell wall.

1.2 Wood-based template

As a raw material, wood is attracting increasing attention because of its unique structure, and excellent mechanical properties,[11] together with low cost and easy processing. Wood products can be processed to different extents with relatively cheap cost. This drives the application of wood as structural material in buildings and furniture. Minimally processed logs are often used in construction. Highly processed wood and wood-based composites have been intensively applied in manufactured for flooring, decking, wood structural panels, boards, joints, or paper industry etc.[12] In the past, the emphasis of wood modification was mainly laid on improving wood properties with regard to shortcomings in practical applications. In some real applications, bleaching of wood is performed to remove brown color from wood veneers used in wood-working and furniture industries. Then, a finishing coating or surface paint is applied.

1.2.1 Native wood

Native wood products generally suffer from dimensional deformation in response to changing relative humidity, susceptibility to biological attack and altering the appearance when exposed to weathering outdoor. This results in shorter lifetime, and limits the application fields of wood.[13] Among these issues, high sensitivity to water is a major problem. Hence, various treatments have been developed to address this. One simple approach is to treat wood by surface coating, for example adding wax on the surface of the wood product.[14] However, such a treatment is not permanent, because the surface coatings may fail by scraping, cracking, or wax may leach out or exude during the lifetime of the product. Failure of coated surfaces is normally due to unfavorable interaction between the coating layer and the wood structure. Surface chemical modification is another approach to improve the compatibility between the

coating layer and wood surface through interfacial reaction. It is of interest to further explore the possibility to bring nanoscale mineral particles or polymers into the cell wall,[15] see wood functionalization in Chapter 1.3. The low specific surface area (SSA) of native wood is a potential problem.

1.2.2 Wood delignification

Although native wood has been successfully used as a template, higher porosity and SSA is needed for applications such as supercapacitor,[16,17] water splitting,[18] etc. Moreover, the penetration behavior of liquid/polymer into wood is strongly dependent on the wood porosity and pore size.[9] Delignification is a beneficial way to tailor the cell wall composition and structure resulting in increased porosity and appearance color changing.[2] The increase of porosity in the cell wall is highly beneficial for the permeability of wood cell wall for wood modification. Extracting lignin while maintaining wood macrostructure is rather challenging because of lignin-carbohydrate complexes.[19] Several methods have been reported for wood delignification with the aims of minimum alternation of wood structure, but removal of the lignin component and/or chromophores from wood tissue.[20–22]

Brogdon et al. reported the chemical extraction of lignin complex components from wood by using an aqueous solution of acetic acid and sodium chlorite in mild conditions.[23] In some cases, chlorite is replaced by sodium hypochlorite.[24] The studies indicate that the aromatic rings from lignin are oxidized by chlorine dioxide generated from sodium chlorite or sodium hypochlorite during the process.[23] Recent chlorine dioxide oxidation investigations show that muconic acid esters and quinones are formed during the reactions. Then, the oxidized lignin structures leach out from the wood structure. In this method, small amount of cellulose and hemicellulose are also removed during the reaction process.

Wood treatment in peracetic acid solution is reported to selectively remove lignin.[25] Under relatively mild conditions, compared to the chlorine dioxide oxidation process, most of the lignin can be removed from wood with only small losses of cellulose and hemicellulose. Both side-chain oxidation and ring cleavage of lignin occur during the process. The side-chain oxidation

proceeds with α-carbonyl formation from a hydroxyl group on the carbon atom α to the aromatic ring. Degradation of vanillyl alcohol by peracetic acid results in ring cleavage and formation of muconic acids as well as side-chain oxidation. Lignin degradation by the white rot fungi is also reported but with damaged and loose wood structure.[26]

Lignin content varies amongst the different layers in the cell wall structure, e.g. secondary cell wall, middle lamella and cell wall corner. Further work is needed for detailed understanding of the cell wall structure change during wood delignification in order to obtain homogeneous delignification inside thick wood samples.

1.2.3 Lignin-retaining bleaching

Lignin accounts for around one third in wood solid content and stabilizes the cellulose. Thus, lignin removal from wood will result in low mechanical strength. Compared to the delignification procedure, lignin-retaining bleaching is used in the production of wood template with higher mechanical performance. It is also better to preserve chemical components of wood by only removing chromophoric goups.[27] This can be achieved by the action of nucleophilic reagents. The lignin-retaining bleaching reagent most commonly used is alkaline hydrogen peroxide. With respect to reactions relevant to selective chromophore removal, studies using simple model compounds have shown that α-carbonyl structures undergo the Baeyer Villiger oxidation to hydroquinones and quinones.[27] The chromophoric groups may also be removed by reductive nucleophilic processes.

1.3 Functionalization of wood

Although wood has been widely used, it still has a number of disadvantages such as dimensional instability from moisture, susceptibility to biological attack and weathering. To overcome these problems, modification methods have been developed that aim at reducing the water accessibility of the cell wall. The possibility is to modify and functionalize wood substrates at the molecular and nanoscale level and thereby control and improve macroscopic properties. Functionalization of wood considered for tailoring

specific functions can also be used in the practical applications.[15,28–30]

1.3.1 Cell wall chemical modification

The principle of cell wall modification is to impregnate a chemical reagent into the cell wall where reaction occurs. As a result, either the groups of wood component are modified or a composite is formed through physical interaction or chemical bonding. The molecular size of the impregnate should be small enough to gain access to the cell wall interior. By being able to specifically functionalize wood in the cell walls, one can add new properties, such as UV-stability, hydrophobicity, fire-retardancy and pH-sensitivity. The wood template should be activated with an initiator or be swollen by the impregnation phase in the wet state (Figure 1.4). The reaction of the chemical agent can occur following two main mechanisms:[2]

i) Monomer or oligomer impregnation (small soluble molecules), with subsequent polymerization /functionalization within the cell wall.

ii) Diffusion of a soluble solution into the cell wall, with subsequent precipitation of inorganic particles in the cell wall (mineralization).

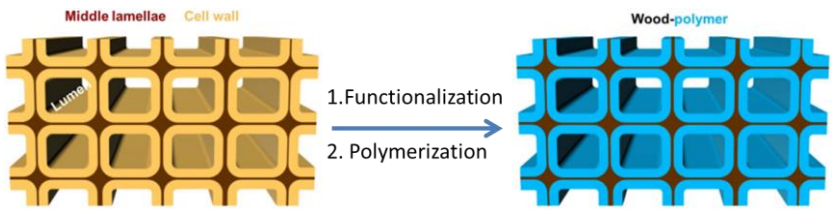

Figure 1.4 Schematic illustration of the basic concept of wood cell wall modification. The wood cell walls are functionalized by grafting polymer chains within the bulk wood structure.[31] (Copyright © 2016 permission from Dr. Etienne Cabane)

For the first strategy, a liquid monomer is introduced into wood scaffold nano- and micro- structures.[32] The monomer is further polymerized so as to be covalently attached to the wood cell wall for achieving a stable functionalization without leaching or unbound chemicals (Figure 1.4).[33] The following have been used: methyl methacrylate, glycerol methacrylate, styrene, flavonoids and furfuryl alcohol.[34,35] Some other examples are based on

resin treatment, such as urea–formaldehyde,[13] phenol–formaldehyde,[36] melamine–formaldehyde,[37,38] and dimethyloldihydroxyethyleneurea.[39,40] This method intends to improve wood dimensional and moisture stability, mechanical properties, biological stability and hydrophobicity.[41–44]

Recently, wood mineralization concepts have been used for multi-functional hybrid organic-inorganic materials based on the second strategy.[15,45–50] Such hybrids can exhibit extraordinary performance in terms of mechanical properties, thermal resistance, fire retardancy, barrier effects and ultraviolet resistance.[51–54] For instance, Merk et al. prepared fire retardant hybrid wood using a bio-inspired mineralization process based on the synthesis of $CaCO_3$ inside the cell walls.[45] Impregnation using silicon-containing compounds is also suggested to achieve silicon/wood hybrids or ceramics.[55–57] Treatment of wood with tetraalkoxysilanes followed by hydrolysis and curing will result in wood impregnated with SiO_2 sol-gel networks. The synthesis of wood-based SiC ceramic was by the carbothermal reduction of wood with silica in acidic conditions.[58]

1.3.2 Lumen impregnation

If the impregnant molecules are incompatible or too large to penetrate into the cell wall, this will result in formation of bulk material in the lumen spaces preventing ingress of agents (Figure 1.5). Keplinger et al. reported a simple two-step strategy to form the stimuli-responsive hydrogels within the cell lumen space.[59] Wood substrate was modified by double bonds which acted as anchor points for functionalization with anhydride. In the second step, the hydrogel molecules were attached to the anchor points. (Figure 1.5) Hydrogels or nanoparticles in lumen offer new functionalities for various applications, for example temperature sensors. In another case, Pd nanoparticles were attached on the cell wall surface for wastewater treatment.[60] Generally, filling of the lumen may block the path available for moisture/water access to cell walls, thereby decelerating the moisture sorption for improved dimensional stability and biological durability of wood.[2]

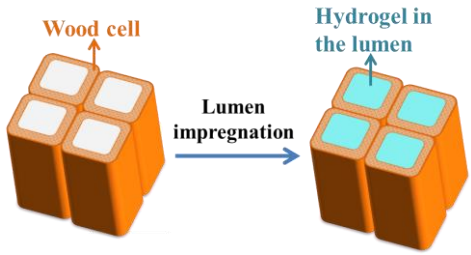

Figure 1.5 Scheme of the lumen functionalization processes. The hydrogel is formed within the lumen of the cells to provide new functionality.

1.3.3 cell wall and lumen functionalization

Another approach is cell wall and lumen functionalization. The impregnant is not only infiltrated into the cell wall but also in the lumen spaces as shown in Figure 1.6. This prevents accessibility of the water, thus preventing biological attack by micro-organisms and improving the mechanical properties. Dong et al. reported in-situ generation of organic-inorganic hybrid polymer within wood through a sol-gel approach (Figure 1.6). A three-dimensional (3D) structure of polymer-SiO_2 hybrids is formed in the native wood template (Figure 1.6a and b). After polymer-SiO_2 sol-gel fixation, the hybrid polymer-SiO_2 3D structure fully fills up wood cell wall and cell lumen (Figure 1.6c and d), and is grafted onto wood components with improvement of mechanical properties, dimensional stability, and decay resistance.[61]

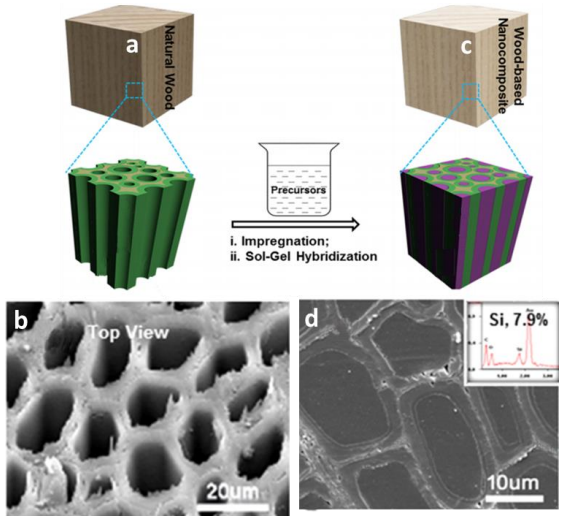

Figure 1.6 Schematic illustrations of natural wood and the wood nanocomposite based on cell wall and lumen functionalization. (a) 3D native wood. (b) Cell wall morphology of the native wood. (c) 3D polymer-SiO_2 wood-based nanocomposite. (d) Polymers are impregnated into cell wall and in the lumen space.[61] (Copyright © 2017, American Chemical Society)

The accessible porosity in the ultrastructural cell wall is correlated to the swelling of wood cell walls.[62] Only limited void space is accessible in the cell wall. Thereby, Yano et al. suggested to initial removal of lignin from veneers based on sodium chlorite delignification treatment.[63] These veneers were then subjected to a low molecular weight phenolic resin impregnation and compression after parallel lamination. The Young's modulus was as high as 62 GPa parallel to the fiber direction.[64] In another study, Fink demonstrated transparent wood by treating wood with a 5% aqueous solution of sodium hypochlorite to remove lignin from wood substances, followed by infiltration of polymer mixture with refractive index matching.[65]

2. Thesis objectives

Materials tend to be either structural or functional, but wood offers the potential to combine the two features in a bio-based material. The focus is on wood-based and transparent wood materials combining both aspects. The objective of this thesis is to prepare porous wood templates/scaffolds, and investigate their characteristics and suitability for transparent wood materials. Transparent wood for engineering purposes is a new topic, and important questions are related to the role of the pretreated template, and efforts to control anisotropy of optical and mechanical properties. In addition, the objective is to consider other possibilities with these templates, specifically the possibility to impregnate the cell wall with clay nanoparticles for the purpose of fire retardancy improvement, and cell wall impregnation by epoxy resin for the purpose of oil/water separation and improved hygromechanical performance. The basic scientific objectives are primarily related to preparation, structure and properties of nanoporous wood templates, understanding of modification mechanisms and structure-property relationship in the modified wood materials.

Wood nanotechnology is the technology to modify wood at nanoscale for engineering purposes. The cases investigated in the present thesis provide encouraging insights with respect to the general potential of wood nanotechnology.

3. Experimental Methods

A brief summary of material preparation and characterization techniques is shown in this chapter. More details are available in the appended papers I to V.

3.1 Materials and chemical compounds

Balsa wood (*Ochroma pyramidale*; density around 150-250 kg m^{-3}; purchased from Wentzels Co. Ltd., Sweden) were prepared with different sizes: 20 × 20 × 1 mm^3 (small size, l×w×t), 20×5×5 mm^3 (medium size, l×w×t) and 50 × 50 × 5 mm^3 (large size, l×w×t), and dried in oven at 105±3 °C for 24 h. For 20 mm × 20 mm sample, different thicknesses were used 0.6±0.1 mm, 1.0 mm, 1.5 mm, 2.5±0.1 mm, 5.0 mm, and 8.0 mm. Pine (*Pinus Sylestris*; density 510 kg m^{-3}), Birch (*Betula*; density 650 kg m^{-3}), and Ash (*Fraxinus excelsior*; density 680 kg m^{-3}) are supplied from Glimakra of Sweden AB. The dimensions are 20 × 20 × 1.5 mm^3 (l×w×t) and 50 × 50 × 1.5 mm^3 (l×w×t).

Chemicals for wood delignification: Sulfuric acid (Sigma Aldrich, H_2SO_4 72 wt%); Peracetic acid (Sigma Aldrich, $C_2H_4O_3$); Sodium chlorite (Sigma Aldrich, $NaClO_2$). Acetic acid (VWR Chemicals, 96 wt%) and sodium acetate (Fisher Chemical, CH_3COONa) were used to prepare acetate buffer with a pH 4.6. Acetate buffer solution was used for chemical extraction process.

Chemicals for wood bleaching treatment: Sodium silicate (Fisher Scientific UK, Na_2SiO_3), sodium hydroxide solution (Sigma-Aldrich, NaOH,), magnesium sulfate (Scharlau, $MgSiO_4$), Diethylenetriaminepentaacetic acid (Acros Organics, DTPA) and then hydrogen peroxide (Sigma Aldrich, H_2O_2)

were used for bleaching wood treatment.

Chemicals for transparent wood preparation: Methyl methacrylate (Sigma Aldrich, MMA); 2,2′-azobis (2-methylpropionitrile) (Sigma Aldrich, AIBN); Aluminium Oxide (Sigma Aldrich, Al_2O_3).

Chemicals for functional wood: Montmorillonite (Cloisite Na+, density of 2.86 g cm^{-3}, MTM) is provided by BYK Instruments (Germany). Bisphenol A Diglycidyl Ether (abbreviated in DGEBA) was bought from TCI chemicals. Jeffamine D-400 polyetheramine (PEA) was provided by Huntsman, USA. Quantum dots (QD, CdSe/ZnS with emission peak around 530 nm) were supplied by Mesolight Inc with a concentration of 25 mg/ml.

3.2 Preparation of functional wood materials

Sodium chlorite delignification: The dried balsa wood samples were treated using 1 wt% of sodium chlorite with acetate buffer solution (pH 4.6) at 80 °C.[66] The reaction time for samples with thicknesses below 3 mm was 6 h and was 12 h for samples with larger thicknesses of 5 and 8 mm. The delignified samples were carefully washed with deionized water and kept in water until further use.

Wood template pressing: Then delignified wood samples were freeze-dried and compressed at 75 kN for 25 min under 25 °C. These compressed delignified wood samples were used for preparation of transparent wood with different cellulose volume fraction.

Delignification based on peracetic acid (PAA) treatment: The wood samples were treated by 4 wt% PAA at 80 °C. The reaction time varies depending on the size of the sample. The samples were treated for 3 h, 6 h and 12 h for small, medium and large size, respectively. Every 6 h fresh PAA solution was changed for large size sample. The extracted wood samples were completely washed using deionized water. The samples were dried by three different methods. Part of delignified wood samples was solvent exchanged by ethanol, acetone and tur-butanol followed by freeze-drying. Part of delignified samples was dehydration by 96 % ethanol and pure ethanol overnight and

then dried by supercritical drying in carbon dioxide.[67] Part of samples was dried by direct freeze-drying.

Lignin-retaining bleaching of wood: Bleaching solution was prepared by mixing chemicals in the following order: deionized water, sodium silicate (3.0 wt%), sodium hydroxide solution (3.0 wt%), magnesium sulfate (0.1 wt%), DTPA (0.1 wt%), and then H_2O_2 (4.0 wt%). Bleaching was accomplished by immersing wood substrate in the bleaching liquor at 70 °C until the wood became white. After bleaching, the samples were thoroughly washed with deionized water and kept in water before the next step.

Clay impregnation: A 2.6 wt % Montmorillonite (MTM) suspension was prepared by strong stirring using Ultra Turrax blender (IKA, DI25 Basic) at 25000 rpm for 20 min followed by sonication using Vibra-cell (Sonics and Materials, Inc.) for 8 min. Then, the clay aggregates were removed by centrifugation at 4500 rpm for 20 min.[68] This procedure was repeated three times, yielding a stable 2 wt % MTM suspension. The delignified wood samples (PAA treated) were solvent exchanged by using ethanol and acetone solution three times for each process before clay impregnation. The native and delignified wood samples were dipped into the MTM suspension, and low vacuum (0.3 bars for 2 h) was performed at the same time. Subsequently, the wet clay impregnated samples were frozen in the fridge overnight at -20 °C and then freeze dried.

Delignified wood/epoxy composite preparation: The porous delignified wood ($NaClO_2$ treated) structure was impregnated with 5 wt% of epoxy/acetone solution (the ratio of DGEBA:PEA was 65:35, w/w) according to the method reported previously.[69] The epoxy solution was impregnated into wood template by using 0.3 bar vacuum for 30 min. These impregnated samples were polymerized under stepwise increasing in oven, 30 °C, 60 °C and 90 °C for 3h respectively, then followed by curing at 120 °C for 12h. The cured template samples were completely washed by acetone twice for removing extra epoxy.

Transparent wood preparation: Before polymer infiltration, wood samples were dehydrated with ethanol and acetone sequentially. Each solvent

exchange step was repeated 3 times. MMA monomer was first pre-polymerized at 75 °C for 15 min with 0.3 wt% AIBN as initiator and then cooled down to room temperature. Subsequently, the delignified or bleached wood templates were fully vacuum-infiltrated with pre-polymerized PMMA. Vacuum infiltration was repeated 3 times to ensure the full infiltration. Finally, the infiltrated wood was sandwiched between two glass slides, packaged in an aluminum foil, and then cured in an oven at 75 °C for 4 h.

Transparent plywood (TPW) preparation: The pre-polymerized PMMA and infiltration processes were performed following TW preparation method. The impregnated delignified five veneers are then assembled with their grains perpendicular (0/90/0/-90/0, cp-TPW) to each other or twisted by increased 45 degree (0/45/90/-45/0, qi-TPW). The polymerization process was completed by oven heating the laminated wood at 70 °C for 4h. The laminated wood was placed between two glass slides and wrapped with aluminum foil. For QD-TPW preparation, wood template were infiltrated with QD in toluene solution before PMMA infiltration.[70] The following process similar to that of luminescent TPW was obtained following similar procedures as cp- and qi-TPW preparation.

3.3 Characterization methods

Field-Emission Scanning Electron Microscope (FE-SEM): The surface cross and modified wood samples were characterized with FE-SEM (Hitachi S-4800, Japan) using an accelerating voltage of 1 kV at a working distance of 3-8 mm. SEM samples were prepared by fracture in liquid nitrogen. All the samples were coated with platinum-palladium prior to FE-SEM observation.

Energy-dispersive X-ray spectroscopy (EDX): Elemental analyses of native-balsa-clay and delignified-balsa-clay cross-section's surface were carried out using an EDX detector equipped in FE-SEM (Oxford Instruments, X-MAX N 80, UK) with accelerating voltage of 15 kV and a working distance of 15 mm.

Lignin content determination and sugar analysis: The lignin (Klason lignin) content of wood samples was measured according to the TAPPI

method (TAPPI T 222 om-02).[71] 200 mg wood sample (40 meshes) were dissolved in 3 ml 72 wt % H_2SO_4 at low vacuum for 1 h followed by the addition of 84 ml of Mill Q water. The solution was hydrolyzed in autoclave at 120±5 °C for 1 h. After that, the precipitate and hydrolyzed solutions were separated by filtration with a glass microfibers filer. Finally, the hydrolyzed solution was diluted to 3 % v/v H_2SO_4 solution for sugar analysis on a Dionex ICS-3000 high performance anion chromatography instrument. The amounts of cellulose and hemicellulose were determined from sugar analysis result. The precipitate (Klason lignin) was dried in the oven at 105±3 °C for 24 h. The lignin content was determined by following equation (1).

$$\text{Lignin } \% = M_l/M_s \times 100\% \quad (1)$$

Where M_l (mg) is the mass of precipitate (lignin) and M_s (mg) is the originally dried mass of the wood sample.

Cellulose volume fraction of TW: Delignified wood essentially consists of holocellulose (cellulose and hemicellulose). The holocellulose volume fraction of TW can be determined by equation (2) and equation (3).[72] For simplicity, we use the term cellulose in the present thesis when we refer to holocellulose.

$$\rho_c = 1/\left(\frac{W_f}{\rho_f} + \frac{W_m}{\rho_m}\right) \quad (2)$$

$$V_f = \frac{W_f \times \rho_c}{\rho_f} \quad (3)$$

Where V_f is the volume fraction of cellulose, ρ_c is the density of composite, ρ_f is the density of holocellulose (1.5 g/cm^3), ρ_m is the density of PMMA, W_m is the weight fraction of the PMMA, and W_f is the weight fraction of cellulose.

Brunauer–Emmett–Teller (BET): Nitrogen physisorption was performed on an ASAP 2020 instrument (Micromeritics) at -196 °C. Wood samples (0.2-0.3 g) were degassed at 70°C for 5 h before the BET specific surface area measurement. The results were collected at a relative pressure between 0.1 and 0.3.[73]

Thermogravimetric analysis (TG, N_2/Air): TG was conducted on a Toledo TGA/SDTA851 instrument. The wood samples (10±1 mg) were placed in the alumina pans and heated from 25 °C to 800 °C with a heating rate of 10

°C/min, in N_2 or air with a flow of 50 ml/min. The TG measurement in air atmosphere was carried out in order to understand the thermo-oxidation performance of the samples, while TG performed in the N_2 atmosphere was discussed the thermal degradation behavior of cellulose in wood/clay composite.

Cone calorimetry: Oxygen consumption cone calorimetry (Fire testing technology, FTT) was used to investigate the combustion of wood samples (50×50×5 mm^3) under a heat flux of 35 kW/m^2. The test was repeated three times for each sample. The following parameters were registered: time to ignition (TTI, [s]), peak of heat release rate (pKHRR, [$kW\ m^{-2}$]) and total heat release (THR, [$MJ\ m^{-2}$]) were evaluated.

Mechanical testing: Tensile tests were carried out on an Instron 5944 with a 500 N load cell, strain rate of 10%/min, and a span of 25 mm. The sample was tracked with an advanced video extensometer. All samples were conditioned for 24-72 h at 50% relative humidity and a temperature of 22 ± 1 °C. Each sample was cut into a strip (5 mm × 60 mm) for testing.

Optical property measurement: The transmittance and haze were measured in a setup containing an integrating sphere. We use a very high brightness light source whose spectrum spans from UV to near-IR wavelengths (170nm - 2100nm) (EQ-99 from Energetiq Technology Inc). For measuring the transmittance, incident beam was first directed into an integrating sphere through one port. Light was directed out of another port of the sphere through an optical fiber, which was recorded by a spectrometer as the WHITE (W) spectrum of the incidence. Haze measurement was done according to ASTM D1003 "Standard Method for Haze and Luminous Transmittance of Transparent Plastics", which is defined as the flowing (Equation 4):[74]

$$\text{Haze} = \left(\frac{T4}{T2} - \frac{T3}{T1}\right) \times 100\% \qquad (4)$$

Where T_1, T_2, T_3 and T_4 are the background checking, total transmitted illumination, beam checking and pure diffusive transmittance, respectively. The size of the specimens is 20 mm × 20 mm. In the measurement, three ports

in the integrating sphere are used; two of them are aligned through the sphere's center allowing transmitted light passing through the sphere without being recorded, and the other one as the signal output port. In this measurement, besides measuring WHITE and DARK, all the SIGNAL spectra are measured according to the position.

The intensity of the scattered light: For the scattering light intensity measurement, a green laser with 550 nm wavelength (4 mm diameter light spot) and was used as incidence. The intensity of the scattered light was measured by an optical power meter. The angle of collection is read from a rotating stage on which the power meter is mounted. The light scattering patterns were taken by using a digital camera (D7000, Nikon). A UV light source (400 nm wavelength) pumped to the luminescent material. Luminescence spectra were measured in a home-built instrument based on an integrating sphere. The selected excitation wavelength was 440 nm (6 nm linewidth) filtered by a monochromator after a laser-driven Xe-lamp.

Small angle X-ray scattering (SAXS) measurement: 2D SAXS measurements were carried out at MAX II storage ring, MAX IV laboratory.[75] The X-ray wavelength is 0.91 nm with sample-to-detector distance of 1885 ± 1 mm. Pilatus 1M is used as the detector with pixel size of 172 × 172 μm^2. 1D scattering profile was extract from the 2D scattering pattern with proper background subtraction and by using DPDAK software.[76]

Wood brightness measurement: The brightness was tested according to ISO brightness 2470-1, 2009.[77] A light source with wavelengths from 170 to 2100 nm was applied (EQ-99 from Energetiq Technology, Inc.).

Attenuated Total Reflection – Fourier Transform Infrared Spectroscopy (AT-FTIR): AT-FTIR was collected using a Perkin-Elmer Spectrum 2000 instrument (Norwalk, CT). The spectrum was recorded over a range of 600-4000 cm^{-1} with a resolution of 4.0 cm^{-1}, and processed using software from Perkin-Elmer Spectrum.

Porosity determination: Porosity was evaluated from the dried mass before and after leaching of the delignified wood/epoxy sample, see in equation 5.[5]

$$\text{Porosity} = (1 - \frac{\rho_t}{\rho_*}) \times 100\% \quad (5)$$

Where ρ_t is the density of the wood template (native wood or delignified wood). ρ_* is the density solid wood. ρ_* is 1570 kg m^{-3} according to the reference.[5]

Contact angle measurement: Contact angles were measured using a CAM-200 contact angle meter (KSV instruments Ltd, Helsinki, Finland) with water as the liquid.

Absorption capacity of water, oil and organic solvent: The absorption capability of water oil and organic solvent is calculated from the following equation (6):[78]

$$\text{Absorption capability (g/g)} = \frac{m_1 - m_0}{m_0} \quad (6)$$

Where m_0 and m_1 are the weights of the sample before and after absorption, respectively. The sample was immersed in the absorbed water or oil for 2-5 min.

4. Wood-based template – preparation and structure

To increase the porosity and facilitate the permeation of the wood cell wall, lignin and/or hemicellulose can be partially removed from the cell wall. In this chapter, chemical extraction of wood based on delignification or lignin modified (bleaching) method is studied (Figure 4.1). The wood template preparation is schematically illustrated in Figure 4.1. Two different strategies are performed: i) lignin is selectively removed from native wood, which is called delignification; ii) chromophore structure is extracted from native wood, lignin is modified in this method, which is called bleaching. The structural details of the obtained material from both chemical extraction routes are compared in this chapter.

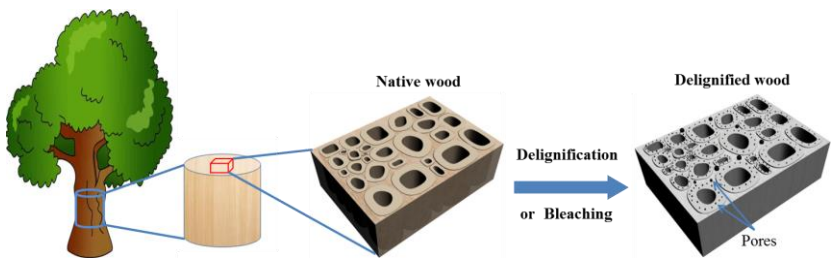

Figure 4.1 Schematic illustration of the preparation of the nanostructured wood template. A nanoporous wood-based scaffold is obtained by removing part of components from the native wood based on delignification or bleaching method.

4.1 Delignification based on sodium chlorite treatment (Paper I and V)

After delignification, the lignin content decreased from 24.9% for balsa

wood to less than 2.9% for the delignified wood, indicating that 88% of lignin is removed. During the process, around 8% reduction of hemicellulose was also observed. This leads to an increase of relative cellulose content in delignified wood (Table 4.1). The skeleton of wood cell wall was well preserved after delignification (Figure 4.2).

Table 4.1 Chemical compositions, SSA, and porosity of native balsa wood and delignified balsa wood based on sodium chlorite treatment.

Samples	Lignin [%]	Hemicellulose [%]	Cellulose [%]	BET SSA [$m^2 g^{-1}$]	Porosity[a] [%]
Native Balsa	24.9±1.4	24.4±1.1	50.7±2.6	1.3±0.2	88.9±1.6
Delignified Balsa	2.9±0.3	16.4±1.4	80.7±2	21±1.1	93.3±1

[a] Porosity values are determined from equation (5) in Chapter 3.3.

The photographs and microscopic morphologies of native wood and delignified wood are shown in Figure 4.2. The native balsa was yellowish before the extraction of lignin (Figure 4.2a). Lignin was extracted by using 1 wt% of $NaClO_2$ in acetate buffer solution (Chapter 3.2). Delignified wood became white in the dry state, indicating that lignin and chromophores were removed from wood (Figure 4.2b). The structure of delignified wood was preserved as shown in the photograph and the microscopic morphology images in Figure 4.2a,b. At submicron-scale, microscale pores were observed in middle lamella and cell wall corner after the removal of lignin (yellow dash in Figure 4.2b). High magnification images revealed nanoscale structure of the cell wall (Figure 4.2). Lignin embedded in the cell walls resulted in a solid S2 layer for the balsa wood (Figure 4.2a). Nanoscale porosity is observed in the secondary wall S2 layer due to removal of lignin (white arrows in Figure 4.2b) leading to 5% increase of porosity (Table 4.1). 2D SAXS experiments were carried out to further characterize the wood nanostructure. 2D SAXS data show 2-fold symmetry anisotropic intensity distribution with a strong streak. The reason is that the preferred orientation of the nanostructured cellulose nanofibers (CNFs) oriented along their long axis parallel to the cell axis.[79] It

means that the cellulose orientation is maintained after the delignification. The increased intensity observable for the delignified wood is due to the increased porosity by lignin removal, which leads to a higher electron density contrast compared to the other wood template components. By extracting the 1D scattering line profile in Figure 4.2e, the intensity in the low q region (<0.4 nm^{-1}), the data for native and delignified wood are observed to show similar trends $I(q) \propto q^{-n}$, with $n \approx 4$ for both horizontal and vertical directions. This indicates a similar structure of the large-scale building blocks with a smooth surface, such as cell wall, in support of preserved wood structure after delignification. Removal of lignin introduces an intensity increase around q= 1.3 nm^{-1}, which corresponds to an increase in the pore size distribution around 4.8 nm via $d=2\pi/q$.

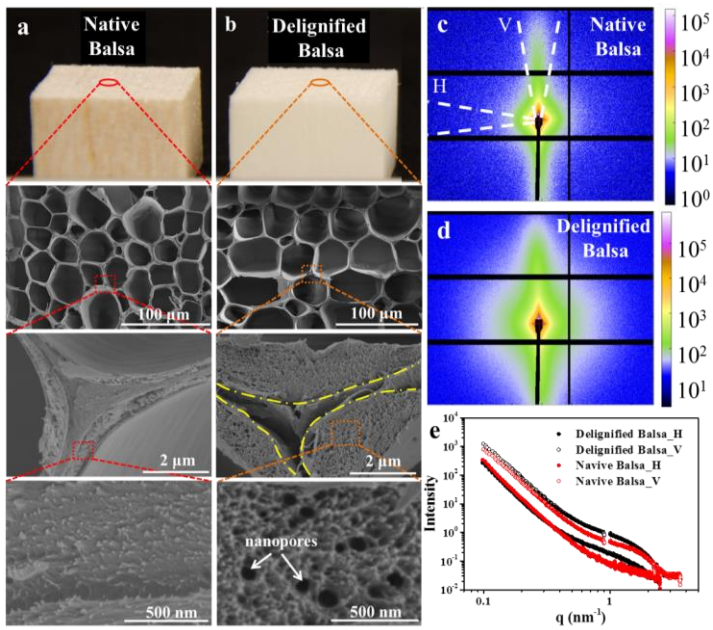

Figure 4.2 Nanoporous structure of wood template: (a) digital photo, low and high magnification cross-sectional SEM images showing the nano structure of native balsa; (b) digital photo, low and high magnification cross-sectional SEM images of delignified balsa wood showing the nanoporosity in the cell wall. 2D SAXS patterns of native balsa (c) and delignified balsa (d). (e)

1D intensity extracted from (c) and (d), the integration regions are illustrated by the dashed lines regions for horizontal direction (H) and vertical direction (V), respectively.

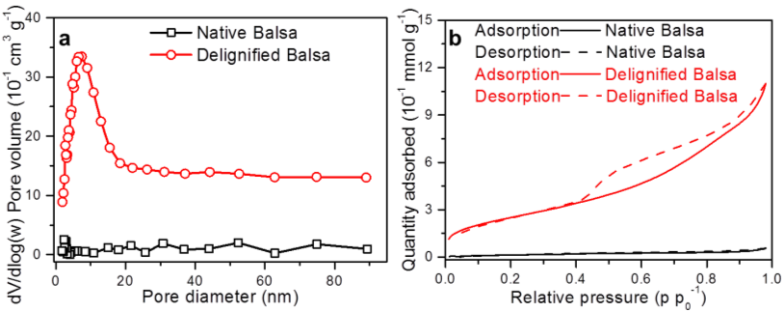

Figure 4.3 a) Pore volume distributions and b) N_2 adsorption/desorption isotherms of native balsa and delignified balsa.

The pore size distribution of the wood structures was examined by BET measurements through physisorption of N_2 (Figure 4.3). A maximum specific surface area (SSA) value of 21 m^2 g^{-1} was obtained after the removal of lignin, whereas SSA values of 1.3 m^2 g^{-1} was obtained for the native balsa. Estimated nanoscale pore volume distributions versus pore sizes in the range of 2–90 nm are compared in Figure 4.3a. The sizes of nanoscale pores in the delignified wood are mainly ranging from 2 to 20 nm (Figure 4.3a). The data are estimated from nitrogen desorption isotherms following the Barrett-Joyner-Halenda (BJH) calculation model (Figure 4.3b). This is similar to data previously reported for delignified spruce wood, which possess pores with sizes in the range of 2–14 nm.[79,80]

4.2 Delignification based on peracetic acid treatment (Paper IV)

For the delignification based on peracetic acid treatment, SEM graphs show that delignification results in nanoscale pore formation in the cell wall and micron-scale pores in the middle lamella (Figure 4.4). The delignified scaffold becomes white with respect to the "native-balsa" (Figure 4.4a). In Figure 4.4b, lignin is rich in the middle lamella (central layer between cells), and dominates at the center of the cell wall corner. In the high-resolution

image (Figure 4.4d), cellulose nanofibrils are apparent as white "dots" sticking out of the surface. They are reinforcing elements embedded in a molecular polymer matrix mixture of lignin and hemicellulose. After delignification, nano- and microscale pores in the cell wall and cell wall corners are apparent (Figure 4.4c,e). The lignin content decreased from 24.9% for native-balsa to 5.5% for delignified balsa (Table 4.2). The hemicellulose content was also reduced. The cellulose mass in the sample was preserved, making the relative cellulose content increased from 50.7 to 74.2% as lignin and part of the hemicellulose were removed. Table 4.2 gives the component weight fractions of balsa wood before and after delignification. If data are expressed as a reduction in the lignin and hemicellulose mass, delignification removed 85% of the lignin and more than 40% of the hemicellulose. The remaining lignin and hemicellulose are important to provide the necessary mechanical robustness to the scaffold.

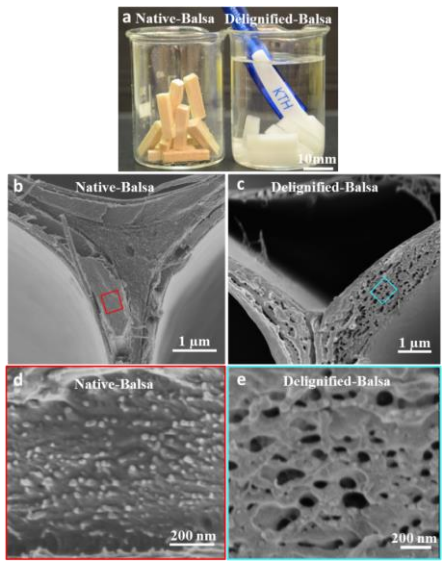

Figure 4.4 Photograph and SEM micrographs of the native-balsa and delignified-balsa scaffold. (a) Digital photograph of the untreated native-balsa (yellow) and delignified-balsa (white). (b) and (c) are at low magnification cross-sectional SEM images of native balsa wood and delignified balsa scaffold. (d) and (e) are high-resolution SEM images of the cell wall S2 layer in

the native balsa wood and delignified balsa wood.[81]

Table 4.2 Composition of native wood (native balsa) and delignified balsa.

Sample	Lignin [%]	Hemicellulose [%]	Cellulose [%]
Native Balsa	24.9	24.4	50.7
Delignified Balsa	5.5	20.3	74.2

The change of the specific surface area (SSA) was evaluated by the BET analysis of N_2 adsorption (Figure 4.5). It should be noted that drying of nanocellulosic structures tends to change the original structure, as well as reduces the porosity and SSA.[67,82] Thus, various drying procedures were used to check the preservation of the structure. The SSA of the delignified-balsa significantly increased compared to those of the native balsa (1.4 m^2/g). The SSA values of delignified balsa wood range from 9 to 41 m^2/g depending on the dehydration and drying methods (Figure 4.5a). The two higher SSA values obtained are from supercritical drying and organic solvent exchange. This can be ascribed to the lower surface tension of both CO_2 gas and organic solvents, so that the pore structure is better preserved.[67] By contrast, drying from water (delignified-balsa) leads to agglomeration of CNFs during the drying process and reduced SSA. Effects from different drying methods are also observed in the nitrogen adsorption− desorption isotherm data (Figure 4.5b). Compared to the sodium chlorite delignification method, PAA treatment has higher SSA and short delignified time. The sample treated with sodium chlorite has higher mechanical property due to high cellulose content. It is also reported that anionic CNF surface charges are obtained after PAA delignification.[83]

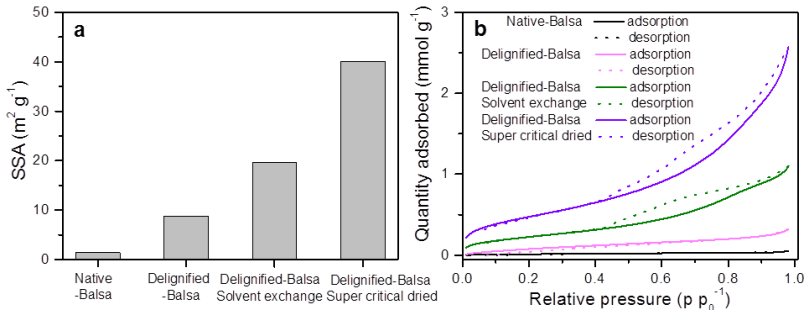

Figure 4.5 (a) BET SSA data of delignified wood after different drying methods. (b) Nitrogen adsorption–desorption isotherms of materials subjected to different processes. Delignified balsa wood was freeze dried. Delignified balsa/solvent exchange was prepared by solvent exchange (ethanol, acetone and tert-butyl alcohol) followed by freeze-drying. Delignified balsa/supercritical drying was achieved by organic solvent exchange (pure ethanol) followed by supercritical drying (CO_2).

4.3 Lignin-retaining bleaching based on alkaline H_2O_2 treatment (Paper II)

Lignin, accounting around 30% of wood, is important for mechanical strength by keeping the integration of cell wall skeleton.[84] Figure 4.6 shows the principle of lignin-removed and lignin-retaining reactions, as well as presents two typical lignin structures, conifer aldehyde and aromatic ketones.

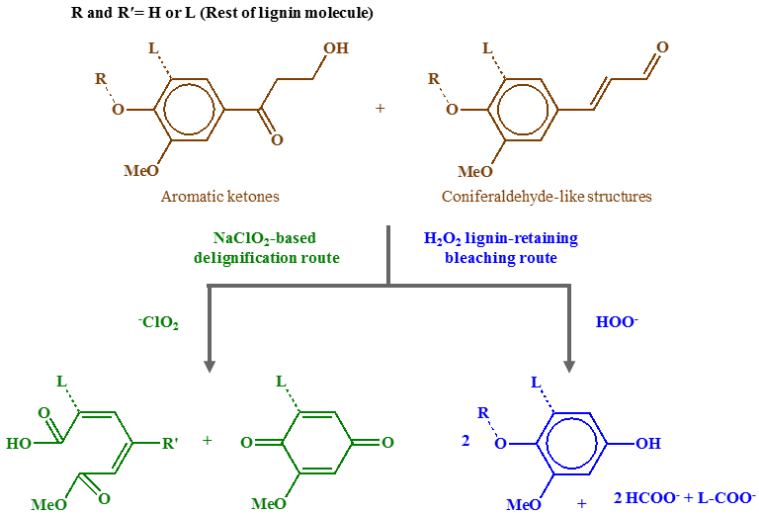

Figure 4.6 Representative lignin reactions and structures contributing to wood color, as well as the main products of the two routes ($NaClO_2$-based delignification and alkaline H_2O_2-based lignin modification).

A comparison between lignin-removed method and lignin-retaining method is presented in Figure 4.7 and Table 4.3. The lignin modification method is completed in a short time (Table 4.3). When wood was exposed to alkaline H_2O_2 treatment, the wood brightness increased from 35% to 77% after only 0.5 h. After 1 h, the brightness reached 79%. For the delignification method, in contrast, the brightness increased slowly with treatment time. The brightness stabilized at around 80 % after a 6 h process. The appearance of the wood template is similar to the previous sample (Figure 4.7 a). In the FTIR spectrum, the band at 1505 cm^{-1} is characteristic of aromatic compounds (phenolic hydroxyl groups) and is attributed to aromatic skeleton vibrations from lignin (Figure 4.7b). There was no intensity decrease around 1505 cm^{-1} in the spectrum, which means lignin was largely preserved. Lignin is photoluminescent and can be excited with UV and visible light with a broad luminescent emission range,[77] whereas polysaccharide components in the cell walls are nonfluorescent. The lignin in the original sample shows a broad luminescent spectrum with a peak around 520 nm (Figure 4.7c). A similar broad photoluminescence spectrum was obtained from lignin-retaining wood.

The peak showed a blueshift, perhaps due to a change in lignin structure during the treatment. The luminescence intensity decreased only slightly compared to the original wood. This also shows that lignin was mainly preserved in the wood structure. For delignified wood, the luminescence spectrum was also obtained due to the lignin residues. However, the intensity was obviously decreased, owing to the lignin removal.

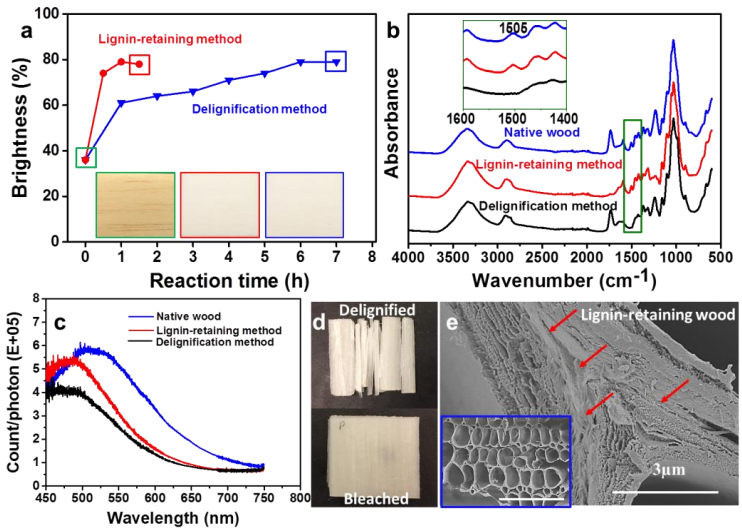

Figure 4.7 (a) Wood brightness before and after lignin modification and delignification; inset images are the photographs of the original wood (left), delignified wood template (middle), and lignin-retaining wood template (right). (b) FTIR spectra and (c) photoluminescence spectra for native wood, lignin-retaining wood template, and delignified wood template. (d) Pine templates with dimensions of 20×20×1.5 mm^3 obtained through delignification (top) and lignin modification (bottom). (e) SEM images of cell wall structures of lignin-retaining transparent wood. The inset images are low-magnification SEM images with scale bars of 100 μm. Red arrows point to the lignin-rich middle lamella.

The lignin content with the lignin modification method decreased only slightly, from 23.5 wt % to 21.3 wt %. Up to 80 wt % (relative value) of the lignin content of the original wood was preserved (Table 4.3). With the

delignification process, the lignin content was decreased significantly from about 23.5 wt% to 2.5 wt%, that is, more than 90 wt% (relative value) of lignin was removed. Lignin-retaining treatment is better to preserve pine structure than sodium chlorite treatment (Figure 4.7d).

Figure 4.7e is the FE-SEM image of the cell wall after H_2O_2 treatment. The cell wall structure was preserved, even in the lignin-rich middle lamella (red arrows). Delamination of the cell wall occurred at the middle lamella to a very limited extent. This is in accordance with preserved lignin distribution. In contrast, cell wall delamination occurred after delignification (Figure 4.2b). Cell walls become separated and the open space between them is much larger than the space originally occupied by the middle lamella. This occurs as the large lignin fraction in the middle lamella, between wood cells, was removed. The weight loss measurement confirms better preservation of the wood composition for all wood species (Table 4.3).

Table 4.3 Comparison of two strategies (delignification and lignin-retaining bleaching methods) and published work[85,86] to prepare the wood templates from various wood species.

Wood species	Treatment methods	Time (h)	Weight loss (%)	Lignin content (%)	Wet strength[a] ∥ fiber (MPa)	Wet strength[a] ⊥ fiber (MPa)
Balsa	Lignin-retaining bleach	2	12	21.3	7.9±1.2	0.2±0.09
	Delignification	6	26.4	2.5	6.9±1.3	0.2±0.04
Birch	Lignin-retaining bleach	2	10.6	20.1	14.4±3.3	0.8±0.2
	Delignification	12	25.3	3.3	1.4±0.4	0.07±0.03
Pine	Lignin-retaining bleach	8	25.0	22.3	14.4±2.2	0.1±0.02
	Delignification	18	40.9	5.2	-	-
Ash	Lignin-retaining bleach	4	15.5	22.4	13.9±1.4	0.2±0.05
	Delignification	18	31.1	5.3	0.8±0.3	-
Basswood[85], thickness∥fiber	Delignification and bleach	12	-	~1.5	-	-
Basswood[85], thickness⊥fiber	Delignification and bleach	6	-	~1.5	-	-
Cathay poplar[86]	Delignification and bleach	16	-	-	-	-

'a': For mechanical test, the samples are cut into dimension of 50 mm × 10 mm × 1.5 mm before chemical treatment.

Lignin-retaining wood templates show better mechanical properties in the wet state (Table 4.3). The lignin-retaining treatment method also leads to better preservation of the mechanical integrity. Lignin is a water-stable bonding element for cellulose fibrils and hemicellulose in the cell wall, and contributes to mechanical properties. After delignification, the mechanical strength of the wood template was significantly reduced. However, with the lignin modification method, this is not a problem. Figure 4.7d shows collapse of the pine samples obtained by delignification (top in Figure 4.7d). With lignin-retaining treatment method, in contrast, the wood structure is well preserved (bottom in Figure 4.7d). In $NaClO_2$-based delignification processes, the aromatic structure undergoes oxidative ring-opening reactions to form acidic groups, which make the lignin more soluble in water (Figure 4.6).[87] Alkaline H_2O_2 treatment removes or selectively reacts with chromophore structures, while the bulk lignin is preserved.[88] It is an attractive method since it is environmentally friendly and industrially scalable, and results in strong brightness/brightness stability effects in wood substrate.[89] The typical reactions are outlined in Figure 4.6.

5. Functional wood materials

5.1 Transparent wood (Paper I and II)

5.1.1 Wood transparency

Wood is not optically transparent since it typically contains 30-90% air depending on wood species. As light goes from the solid tissue into lumen space, considerable scattering takes place due to mismatch refractive index between the cell wall and gas (air). In addition, lignin contains chromophores which absorb light. In order to achieve optical transparency, two main problems should be addressed: i) removal of light absorbent – lignin and/or chromophores; ii) impregnation of polymers into lumen spaces, where the polymer has a refractive index similar to the cell wall material. The transparent wood concept is shown in Figure 5.1. Wood can therefore be made transparent through chemical extraction of lignin and/or chromophores followed by polymer infiltration. Transparent wood was first prepared by Fink for the purpose of wood morphology studies.[65] Paper I in the present thesis is then the first study where transparent wood is considered for engineering purpose.[66]

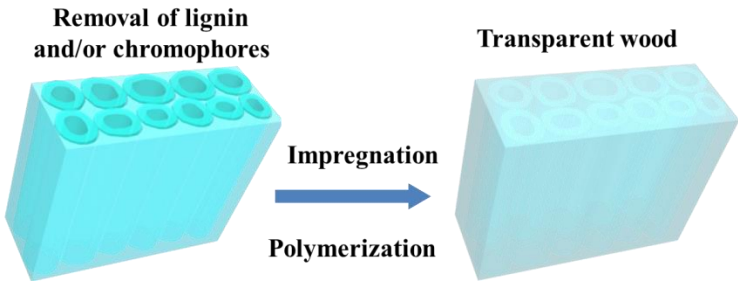

Figure 5.1 Schematic illustration of transparent wood concept, with impregnation of liquid monomer/oligomer mixture followed by polymerization.

5.1.2 Polymer impregnation of wood

Wood is porous and can be impregnated by liquid monomer/oligomer mixtures, by mechanisms related to water transport in wood. The present procedure is described in the experimental section, and is similar to what is used during polymer composites production by vacuum infiltration of porous fiber reinforcements. The microscopic structure of transparent wood is presented in Figure 5.2. Figure 5.2a shows an optically transparent wood sample (1.2 mm thick) positioned on the "KTH" logo. PMMA polymers were impregnated and polymerized in lumen spaces as shown in Figure 5.2b. In the high magnification SEM image of the cell wall cross-section, there is no visual nanoporosity in the cell wall (Figure 5.2c) compared to the delignified wood template (Figure 4.2b in Chapter 4.1). Note that PMMA is present in the lumen, but it is not confirmed to be present inside the cell wall. The nanostructure of cellulose nanofibers was also maintained without much agglomeration or collapse, as is apparent in high magnification SEM images (Figure 5.2d).

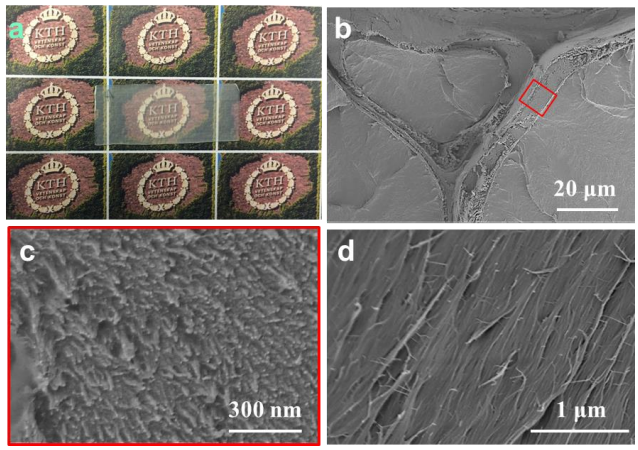

Figure 5.2 The SEM morphology of transparent wood. (a) The optical image of a 1.2 mm thick transparent wood sample with size of 50 mm×20 mm on substrate with text. (b) Low magnification SEM image of transparent wood cross-section showing the presence of PMMA. High magnification SEM image of transparent wood cross-section (c) and transparent wood surface (d) indicate well-preserved cellulose nanostructure.

5.1.3 Properties of transparent wood

The optical properties of transparent wood are presented in Figure 5.3. A high transmittance value of 90% at a wavelength of 550 nm was obtained for a transparent wood thickness of 0.7 mm (Figure 5.3a). The transmittance decreases with increased thickness. When the thickness was 3.7 mm, the transmittance decreased to around 40%. During light transmission in transparent wood, light attenuation takes place primarily to scattering in the material. With different cellulose volume fractions from 5 to 65%, the transmittance decreased from 85% to 35% (Figure 5.3b).

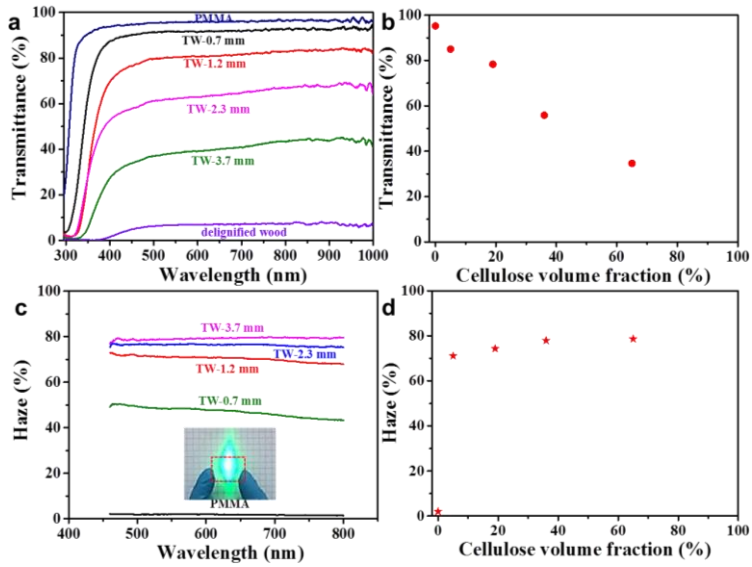

Figure 5.3 Optical transmittance of transparent wood. (a) Transmittance of transparent wood samples with different thicknesses; (b) The dependency of optical transmittance on cellulose volume fraction. (c) Dependency of haze on the thickness of transparent wood. The inset image shows light scattering of the green laser beam with a diameter of 4 mm as it passes through the transparent wood. (d) Effect of cellulose volume fraction on haze, all the samples are around 1.2 mm thick.[66]

Transparent wood possesses high optical haze characteristics as shown in Figures 5.3 c,d. In contrast to transmittance, haze increases with increasing thickness (Figure 5.3.c). The scattering pattern has parallelogram-like shape (insert in Figure 5.3c) due to the anisotropic structure of wood. Figure 5.3d shows that the haze depends on cellulose volume fraction. At a thickness of 1.2 mm, the haze slightly increases with increasing cellulose volume fraction from 8% to 65%.

For transparent wood (TW), mechanical properties are also important, since it may be anticipated to use TW as a building material. Figure 5.4a presents the tensile stress-strain curves of transparent wood. The elastic modulus increases from 2.05 GPa (with a 5% cellulose volume fraction) to 3.59

GPa (with a 19% cellulose volume fraction). This is higher than that for delignified wood. In the high cellulose content (19%) transparent wood, the elastic modulus and tensile strength are twice more than for neat PMMA (Figure 5.4a). The synergy between PMMA and template is ascribed to the mechanical properties of cellulose nanofibers in the template, their orientation, and the favorable interaction between cellulose nanofibers and PMMA. Figure 5.4b illustrates cross-link interface between cell wall and PMMA due to favorable interfacial interaction between modified cellulose/PMMA and the PMMA-rich lumen space. The hierarchical and longitudinally oriented cellulose nanofiber structure not only provides increased modulus, but also provides strength improvement for the transparent wood.

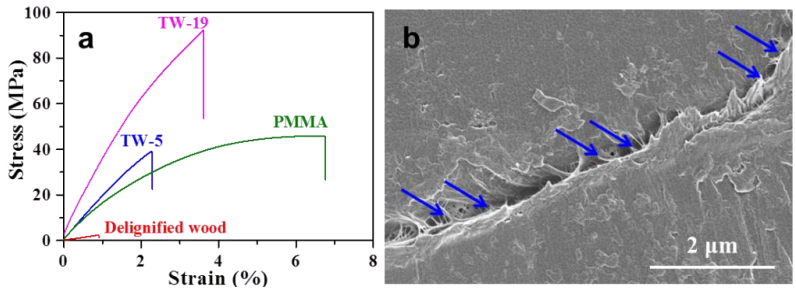

Figure 5.4 (a) Stress–strain curves in uniaxial tension for transparent wood, V_f 0.19 (TW-19) and V_f 0.05 (TW-5), delignified wood and PMMA. (b) SEM micrograph of transparent wood showing the nanofibrous nature of the cell wall region and favorable interaction (bonding) with PMMA.[66]

There are practical disadvantages in making transparent wood from delignified wood templates, since delignified wood is very weak and sensitive to rough handling for softwood. Thus, "lignin-retaining" transparent wood was developed using pine and ash in a bleaching-type of process where lignin chromophores are removed.[90] The optical and mechanical properties of lignin-retaining transparent wood are presented in Figure 5.5. The "Transparent wood" text is visible behind the lignin-retaining transparent wood. The optical transmittance and haze of lignin-retaining transparent wood at 550 nm wavelength were 83 % and 75 % respectively for a specimen thickness of 1.5 mm (Figure 5.5a,b). The "Transparent wood" text is not visible when lignin-

retaining transparent wood is positioned 5 mm above the text paper (insert in Figure 5.5b) due to light scattering as light exits on the back side of the specimen.

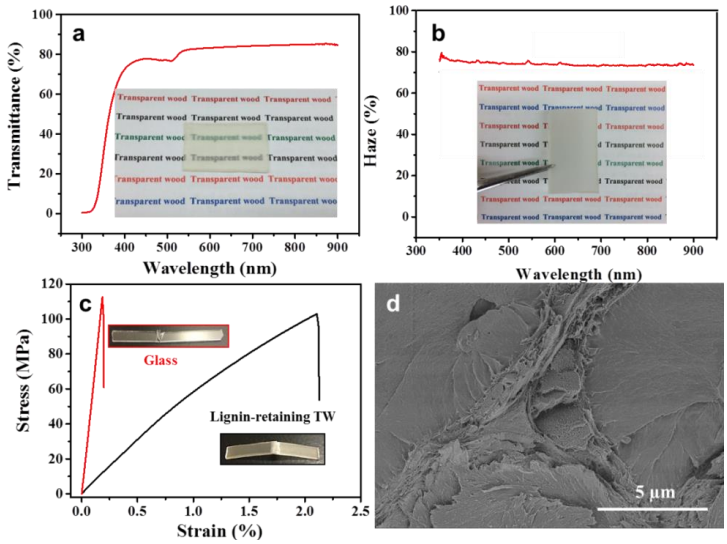

Figure 5.5 a) Optical transmittance of TW-lignin; the inset is a photograph of transparent wood with thickness of 1.5 mm. b) Optical haze of Lignin-retaining TW; the inset is a picture of Lignin-retaining TW with a 5 mm gap between the sample and the underlying paper. c) Three-point bending experiments, estimated stress–strain curves of Lignin-retaining TW and glass; inset images are the fractured samples after test. d) SEM image of Lignin-retaining TW after fracture, demonstrating ductile fracture appearance.[90]

A 3-point bending test was carried out, with resulting stress–strain curves shown in Figure 5.5c. Transparent wood showed comparable stress at break (100.7 ± 8.7 MPa) with glass (116.3 ± 12.5 MPa), but much higher strain to failure (2.18 % ± 0.14) than glass (0.19 % ± 0.02). This leads to one-order of magnitude higher work of fracture for transparent wood (119.5 J m^{-3}) compared with glass (10.2 J m^{-3}). This is due to the reinforcing wood template skeleton in the composite. The wood–PMMA bond integrity appears favorable at sub-micrometer scale (Figure 5.5d), which leads to load transfer in the composites.

Demonstrations using transparent wood as building materials are shown in Figure 5.6. With the combined optical properties, mechanical performance and low thermal conductivity, transparent wood is a good candidate for energy-saving buildings. A transparent wood roof is suggested in Figure 5.6a. The inner space is dark, and artificial lighting is needed for normal wood (Figure 5.6a, center). A transparent wood roof, in contrast, allows light transmission to the interior of the house (Figure 5.6a, right), and can be used in applications where no thermal insulation layer is needed. Moreover, with the transparent wood characteristic of high haze, the indoor privacy is also protected at the same time. By using quantum dots embedded in a transparent wood panel, diffused luminescence is also possible (Figure 5.6b).[70] This could be advantageous for planar light sources and luminescent building construction elements or furniture (Figure 5.6b, right).

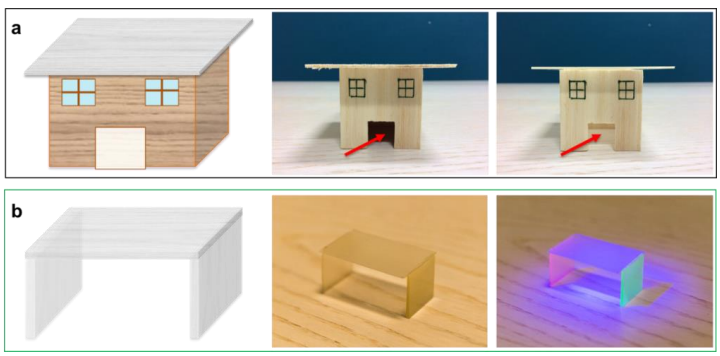

Figure 5.6 a) Design of model house with transparent wood roof. Model house with original wood roof, where indoor is dark. b) Model house with transparent wood roof, where the indoor environment has light entering from outside. Design of transparent wood stool furniture (b, left). Photograph of a piece of luminescent transparent wood stool furniture model.

5.2 Transparent plywood (Paper III)

5.2.1 In-plane isotropic properties

Wood veneer can be considered as an orthotropic material (special case of anisotropy) with different properties in different directions. The mechanical

properties of TW in longitudinal direction are much higher than in the transverse direction. If TW would be used as a load-bearing building material, it would be subjected to multiaxial stress states with a risk for failure in the weak transverse direction. In-plane isotropy is then desirable, in a similar way as for existing plywood structures. Quasi-isotropic composite laminates, with lamellae in the 0°, 90° and +45°, -45° directions can show the same modulus in all in-plane directions.[91]

5.2.2 Lamination

In the present study, two types of lay-ups with either cross-ply lamination (0° and 90° veneer layers termed plies) or close to quasi-isotropic lamination structure are selected, and termed transparent plywood (TPW). Schematic illustration of TPW is shown in Figure 5.7. The delignified templates were first compressed, to increase the cellulose volume fraction. High cellulose volume fraction improves the mechanical properties. The compressed delignified veneers were then impregnated with prepolymerized methyl methacrylate monomer/oligomer mixtures (termed PMMA) and stacked with different orientation angles (Figure 5.7a). In this thesis, five plies were laminated with cellulose orientations in 0/90/0/90/0 degrees (denoted cross-ply TPW, cp-TPW in abbreviation) or in 0/45/90/-45/0 degrees (denoted as quasi-isotropic TPW, qi-TPW in abbreviation) (Figure 5.7 b).

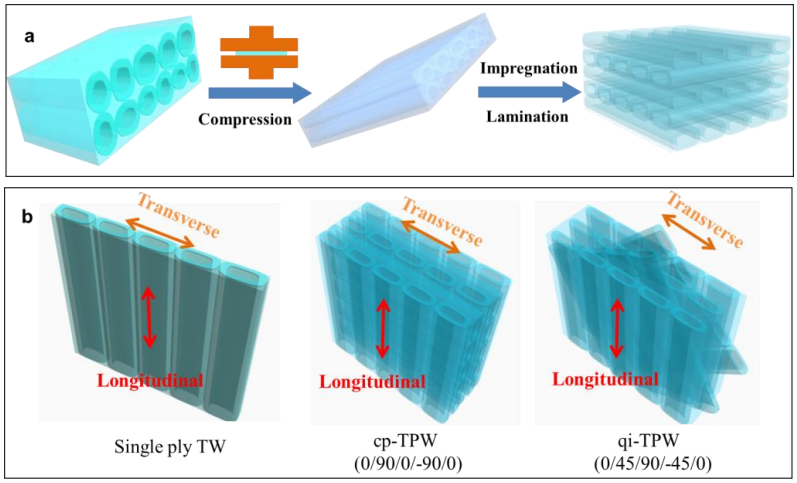

Figure 5.7 Schematic illustration of the preparation processes for transparent plywood (TPW). (a) Compressed delignified wood templates were used. The TPW was fabricated by laminated layers of PMMA impregnated delignified wood. (b) Single ply TW; Cross-ply transparent plywood (cp-TPW) with lamination angles at 0/90/0/-90/0 degrees; Quasi-isotropic transparent plywood (qi-TPW) with lamination angles at 0/45/90/-45/0 degrees.

5.2.3 Laminated structures and properties

The layer and interlayer structures of TPW are presented in Figure 5.8. The wood structure is sandwiched between two PMMA layers for the single ply TW (Figure 5.8a). Figure 5.8b,c show the fracture surfaces (interlayer regions are marked in yellow in Figure 5.8b,c) from cp-TPW and qi-TPW, respectively. Interlaminar interface regions are without apparent micro-scale defects (brownish lines in Figure 5.8d,e).

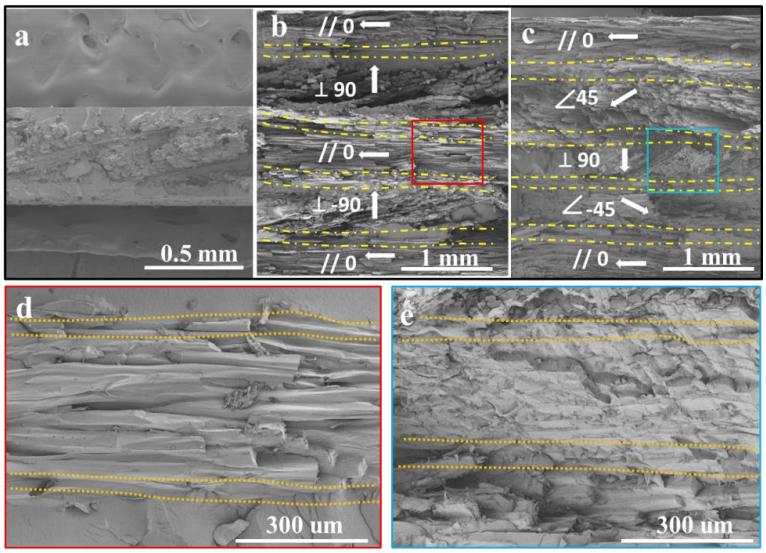

Figure 5.8 SEM micrographs of TPW plywood. a) Single layer transparent wood; b) five-layered transparent plywood in cp-TPW; c) five-layered transparent plywood in qi-TPW; d) high magnification interlaminar region in cp-TPW; e) high magnification interlaminar region in qi-TPW.

The typical tensile stress-strain curves in longitudinal and transverse directions are presented in Figure 5.9. Note that 0 and 90 degrees are defined as longitudinal (L) and transverse (T) directions (Figure 5.7b). The tensile test directions are shown in Figure 5.9a,b. The strength and elastic modulus are around 40 MPa and 2.3 GPa for the pure PMMA (Figure 5.9c). The longitudinal ultimate strengths are slightly higher, 50.1 MPa for cp-TPW and 45.4 MPa for qi-TPW. Compared to PMMA, the elastic modulus increases considerably to 4.1 GPa for cp-TPW and 3.9 GPa for qi-TPW with 10 vol% cellulose (Table 5.1). This increase can be ascribed to cellulose nanofibers as reinforcement element in TPW.

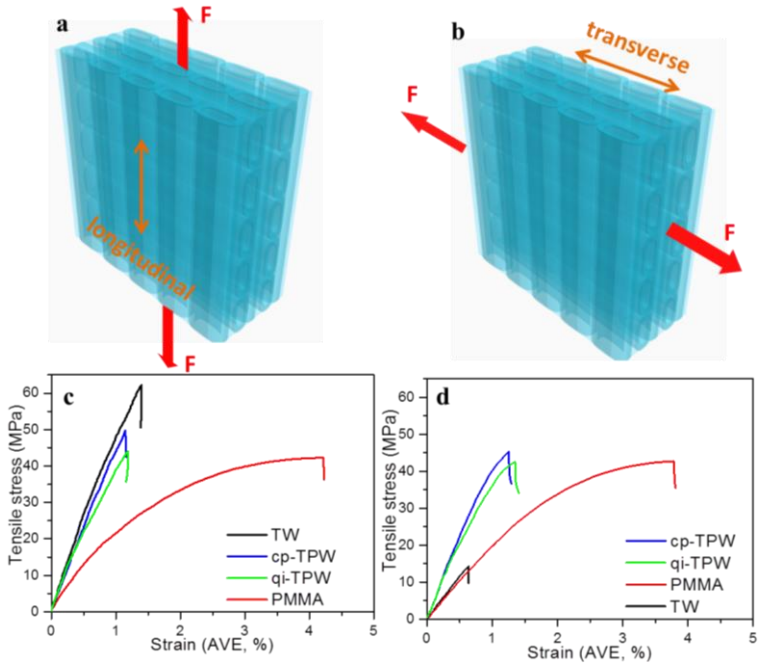

Figure 5.9 Mechanical properties of TPW. Sketches show the loading in a) longitudinal direction and b) transverse direction, respectively. Typical stress-strain curves of the tensile test in c) longitudinal direction and d) transverse direction, respectively. The tensile displacements were traced by optical video technique.

The weakest mechanical properties in the transverse direction are a limitation for many applications. The ultimate transverse strength and elastic modulus were 14.6 MPa and 2.4 GPa for single ply TW (Figure 5.9d and Table 5.1). The ultimate strengths for the two types of TPWs with 10 vol% cellulose are 42 MPa for qi-TPW and 45 MPa for cp-TPW, respectively. Similarly, the "transverse" elastic modulus in T direction increases from 2.4 GPa (single ply TW) to 3.5 GPa for qi-TPW and 3.9 GPa for cp-TPW, respectively. This increase is due to the laminated structure.

Table 5.1 Summary of the mechanical properties of single ply and TPW.

Wood samples	Tensile test direction (L/∥;T/⊥)	Cellulose volume fraction (%)	Size	Mechanical performance*			
			l×*w*×*t* (mm³)	*E* (GPa)	E^a (GPa)	*σ* (MPa)	*ε* ≈ (%)
Single ply TW	L	12	60×5×0.8	4.3	-	62.5	1.5
	T	12		2.4	-	14.6	0.7
cp-TPW	L	10	60×5×3.5	4.1	3.7	50.1	1.2
	T	10		3.9	3.3	44.9	1.3
qi-TPW	L	10	60×5×3.5	3.9	3.4	45.4	1.2
	T	10		3.5	3.0	42	1.4

'-': No data available. 'l×w×t': Length, width and thickness, respectively. 'E': The Young's modulus from the experimental data. E^a: The predicted Young's modulus is determined based on the laminate plate theory. 'σ': Ultimate strength. 'ε': Failure at break. '*': The mechanical performance values were calculated from tensile test with advanced video extensometer (AVE).

The laminated TPW structures provide unique optical characteristics (Figure 5.10). The transmittance for cp-TPW is up to 83%, slightly higher than 75% for qi-TPW at a thickness of 3.5 mm (Figure 5.10a). The transmittances for both TPWs are lower than for single ply TW due to attenuation and scattering in the laminated composite. Figure 5.10b demonstrates high optical haze, about 80% for both types of TPW. Single layer TW displays a haze of around 50%.

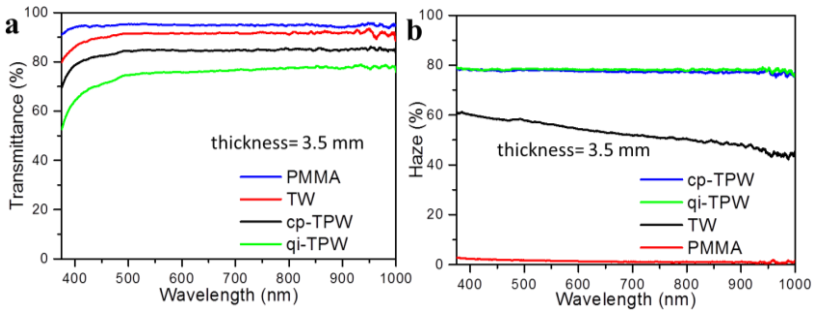

Figure 5.10 Optical properties of the TPW. a) Total transmittance of single layer TW, neat PMMA and TPW; b) Haze for cp- and qi-TPW, single TW and neat PMMA.

The scattering patterns and light intensity at different angles are presented in Figures 5.11a-d. A squeezed parallelogram-like scattering pattern for the single ply TW is presented in Figure 5.11a. The scattered light distribution for single ply TW is substantially different between L and T directions because of the anisotropic structure of wood. In contrast, a circular scattered results for the qi-TPW (Figure 5.11b). The intensities of the scattered light beam show Gaussian-like distributions in both L and T directions (Figure 5.11c,d). The scattered light intensities for TPW spread within a broad range of angles from -60 degree to 60 degrees. The five-layer qi-TPW appears to create an isotropic light scattering effect (Figure 5.11d). For the single ply TW, there is high light intensity at small angles between -10 and 10 degrees (Figure 5.11c).

In addition, quantum dots (QDs) were embedded in the material in order to create a luminescent material. CdSe/ZnS QDs were used, resulting in a lighting panel which emits green light when excited by UV light. The wood templates were impregnated by QD and PMMA oligomers and then laminated into luminescent TPW with isotropic light emitting characteristics, as shown in Figures 5.11e,f. For a single ply anisotropic TW@QD, the luminescence is not uniformly distributed over the sample (Figure 5.11e, left). In contrast, the luminescent light from the transparent plywood "TPW@QD" shows highly scattered uniform illumination (right side in Figure 5.11f), which could potentially be used for luminescent lighting applications.

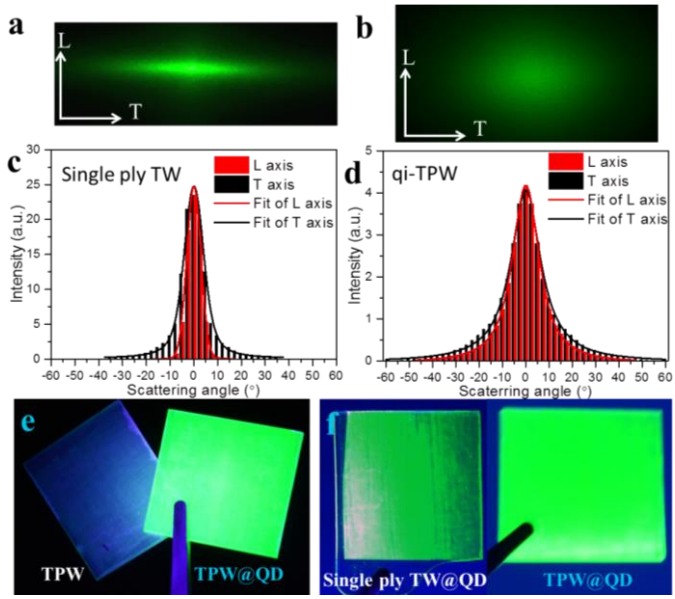

Figure 5.11 Light scattering of the TPW. a,b) Camera images of light scattered by single layer TW and qi-TPW, respectively; c,d) light intensity distributions in x and y directions are shown in (a) and (b) for single ply TW and TPW, respectively. e) TPW and TPW@QDs exposed in vertically incident UV light. f) Single ply TW@QDs and TPW@QDs in UV light.

5.3 Fire retardant wood/clay nanocomposite (Paper IV)

Wood mineralization can be environmentally friendly, and has been used for multifunctional hybrid organic/inorganic materials.[15,30] The "mineralization" can either take place by precipitation of inorganic particles from salt solution, or by simple addition of inorganic particles to the wood material. Inorganic/organic hybrids can exhibit extraordinary performance in terms of mechanical properties, thermal resistance, fire-retardancy, barrier effects, and ultraviolet resistance. An important scientific challenge for functionalization of native wood is that nanoparticles truly become located inside the cell wall. The main present achievement is that a truly nanostructured wood hybrid is prepared based on inorganic clay

nanoplatelets distributed inside the wood cell wall. We are impregnating a delignified and highly nanoporous scaffold with a colloidal suspension so that nanoplatelets are diffusing into the cell wall of the template.

5.3.1 Mechanism for nanoparticle deposition inside cell wall

Based on the study of Chapter 4.2, wood architectures with increased nanoporosity were prepared by delignification based on peracetic acid treatment (Figure 4.4). The delignified scaffold shows porosity on several length scales while preserving its original structure. It may be functionalized in many different ways to extend the property range and functionalities in wood-based composites. As schematically shown in Figure 5.12, the potential for nanoclay diffusion into the cell wall is investigated. The nanocellulosic wood scaffold (Figure 5.12, left) was impregnated with colloidal MTM clay for the purpose of forming a nanostructured wood hybrid (Figure 5.12, right).

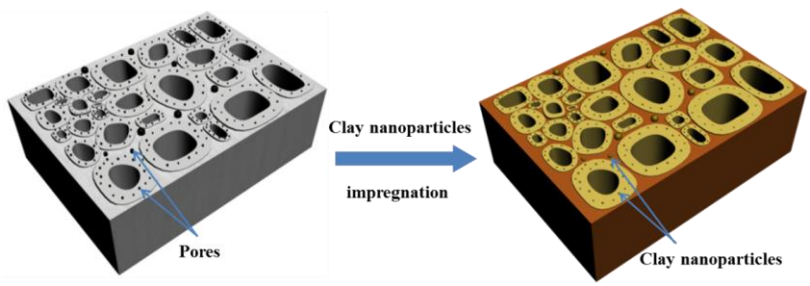

Figure 5.12 Schematic illustration of preparation for the nanostructured fire-retardant wood hybrid. The wood hybrid was formed by impregnation of a nanoclay hydrocolloidal suspension.

5.3.2 Cellular structure and potential clay diffusion into the cell wall

Organic/inorganic wood hybrids were prepared by soaking native wood and delignified balsa scaffolds in a hydrocolloidal clay suspension. After this treatment and drying, the weight percent gain was 4.1% for the native-balsa-clay sample, whereas it was as high as 17.3% in delignified-balsa-clay. The cellular structure of native-balsa-clay samples appears similar to native balsa wood at the micro-scale (compared Figure 5.13a and 4.4b). In high resolution SEM images, pores are observed in the cell wall (Figure5.13b). The lumen

space is empty indicating that the MTM nanoclay content in the lumen is low (insets of Figure 5.13a,c). However, the high resolution cell wall morphologies of delignified balsa clay are completely different as compared with without clay (compare Figure 5.13d and 4.4e). The pores in the cell wall are no longer visible, and the structure appears denser (Figure 5.13d). This is ascribed to the presence of nanoclay particles inside the cell wall; see high magnification micrographs (Figure 5.13c,d). Water or clay/water mixture is absorbed by the delignified cell wall during soaking, and this process may be rapid due to the strong capillary forces expected due to the nano- and micro-scale pores. In order to even out concentration gradients, clay nanoparticles are likely to diffuse into the cell wall so that the clay concentration becomes closer to the concentration of the original colloid. Some of the larger clay nanoparticles may be unable to diffuse into the cell wall.

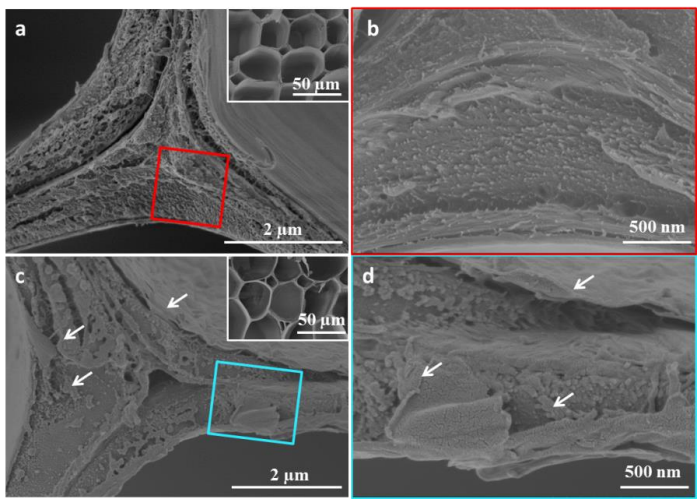

Figure 5.13 SEM micrographs of native balsa clay (a,b) and delignified balsa clay (c,d) samples. The inset SEM images in (a) and (c) are the cell walls of native balsa clay and delignified balsa clay, respectively. The rectangles in (a) and (c) are the positions of the high resolution images in (b) and (d), respectively. The arrows in (c) and (d) indicate suspected location positions of the nanoclay particles.[81]

5.3.3 Confirmation of clay location

EDX spectroscopy of specimen cross-sections was carried out to detect clay location. The relative intensities of the spectrum were collected scanning across the cell wall (yellow line in Figure 5.14a). The signals of silicon and aluminum (orange and yellow in Figure 5.14b) distributed across the cell wall thickness indicate a high concentration of clay nanoparticles inside the cell wall. The nanopore size in the cell wall is important. The results are significant because it may be possible to put arbitrary nanoscale particles inside the cell wall of delignified wood scaffolds. The distributions of the delignified scaffold pore size (from BET data) and clay particle size are shown in Figure 5.14c. The overlap region in 40-90 nm (pink area) indicates that a considerable fraction of the nanoclay is small enough to enter the pore structure in the scaffold. The large size clay particles (larger than 100 nm) are probably not able to diffuse into the cell wall but are deposited on the surface of the cell wall. With respect to mechanisms, some clay may go inside the cell wall already during initial liquid absorption, but the clay platelets may also later diffuse into the liquid-filled cell wall to simply equilibrate any clay concentration gradients.

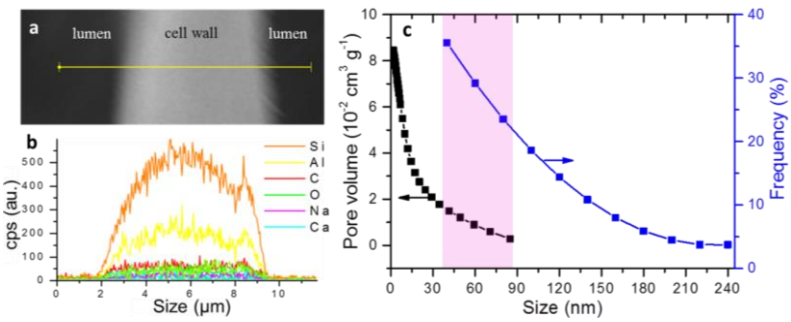

Figure 5.14 Clay particle distribution in the cell wall for the sample of delignified balsa clay. (a) SEM in the line scanning mode; (b) element distribution across the cell wall; and (c) size distribution of clay particles (blue) and pore volume distribution in the cell wall (black) after delignification.[81]

5.3.4 Properties of wood/clay biocomposites

The thermal and thermo-oxidative stabilities of native and modified wood were evaluated by thermogravimetric (TG) analysis in nitrogen and air,

respectively (Figure 5.15). The weights for all samples are initially reduced due to water evaporation. After this stage, the wood components undergo pyrolysis, which occurs in different temperature ranges. Hemicellulose, cellulose and lignin are degraded in the range of 200–260°C, 240–350°C and 280–500°C, respectively.[92–95] The strong decomposition in the range of 250-350°C in Figure 5.15a ascribes to pyrolysis of hemicellulose and cellulose and appears at a temperature corresponding to the maximum decomposition rate,[96] although lignin is certainly also degraded in this range. The following broader temperature range may result in higher char yields is ascribed to lignin decomposition,[94] although oxidation of char from cellulose is also taking place.

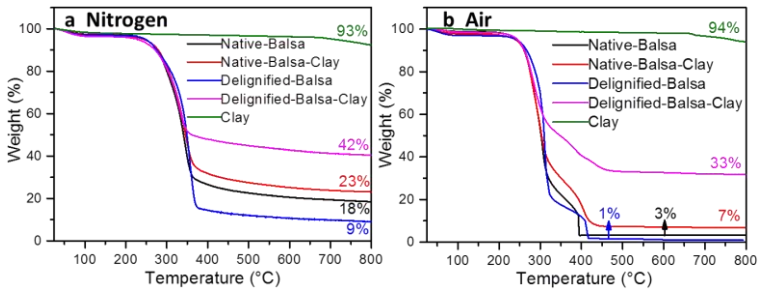

Figure 5.15 TG curves for the native wood and wood/clay nanocomposite hybrids in nitrogen (a) and air atmosphere (b). The values in (a,b) are the final residue weights at 800°C. Note that native balsa clay has a clay content of 4.1 wt% and delignified-balsa-clay has a clay content of 17.3 wt%.[81]

In Table 5.2, it is apparent that delignification increases Tmax for wood template. The reason is the increased crystalline cellulose content.[97] Delignified balsa clay sample shows as much as 42% residue at 800°C. Clay nanoparticles in the cell wall improve stable char formation from 9% to 25% (Figure 5.15a and Table 5.2). The cellulose-clay structure increases the char production of cellulose partly by acting as a thermal insulator and providing Na+ catalytic sites, thereby enhancing degradation paths toward char formation.[98,99]

Table 5.2 Thermogravimetric data for native balsa and delignified balsa/clay hybrids in nitrogen and air.

Sample	Nitrogen			Air			
	$T_{onset10\%}$ [°C]	T^*_{max} [°C]	Residue at 800°C [%]	$T_{onset10\%}$ [°C]	T^*_{max1} [°C]	T^*_{max2} [°C]	Residue at 800°C [%]
Native-balsa	277	345	18	263	304	393	3
Native-balsa-clay	280	342	23	261	301	405	7
Delignified-balsa	272	357	9	267	277	356	1
Delignified-balsa-clay	2 75	330	42	262	285	386	33

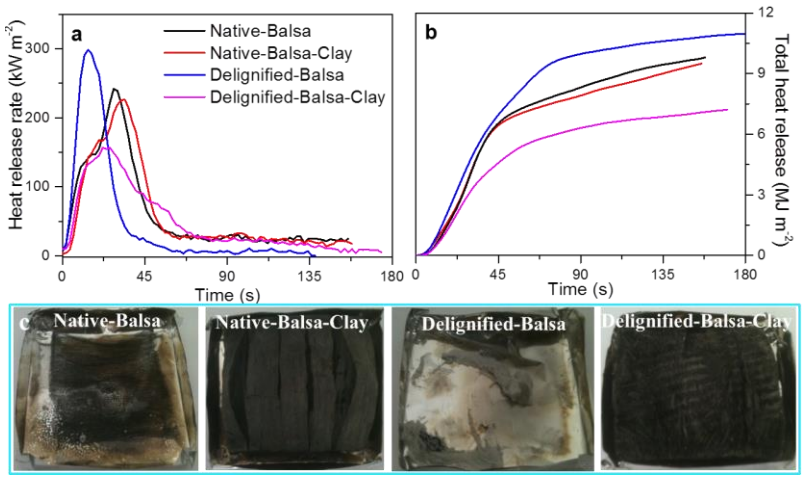

Figure 5.16 Cone calorimetry data of unmodified and modified wood and wood scaffolds: (a) average HRR plots, (b) average THR plots, and (c) snapshots of residues collected at the end of the tests.[81]

Data were also obtained in oxidative environment (in air, Figure 5.15b). After initial char formation, CO and CO_2 are generated from the char residue in the second degradation process.[100] The delignified balsa clay sample reduces degradation kinetics as observable from the curves (Figure 5.15b) and Tmax2 values in Table 5.2. The presence of clay in the cell wall probably slows oxygen

diffusion within the charred residue. The final residue evaluated at 800°C still contains 16% of organic char at 800°C, showing strong contribution from clay to formation of thermally stable structures.

Cone calorimetry was investigated to obtain information about the fire retardancy behavior (Figure 5.16 and Table 5.3). In the early stage, a protected char from lignin is produced on the surface, which reduces the amount of combustible volatiles and the HRR (Figure 5.16a). This protection layer is finally destroyed and there is a sudden increase in HRR which reaches its maximum value (pKHRR=245 kW/m^2) for native balsa. No protective surface char is generated for delignified balsa samples and the HRR plot steeply reaches its maximum value which is higher than for native balsa (296 vs 245 kW/m^2 as reported in Table 5.3). The clay-containing material shows much better properties. HRR is strongly reduced to a smaller value (157 kW/m^2) with the protection of a clay barrier layer. The increase in THR of all wood specimens is almost linear between 5 to 40 s, and then it levels off (Figure 5.16b). The presence of clay reduces the THR due to the thermally stable char.

Table 5.3 Cone calorimetry data of unmodified and modified samples.

Sample	TTI [s]	pKHRR [kW m^{-2}]	THR [MJ m^{-2}]	SPR [10^{-4} m^2 s^{-1}]	TSR [m^2]
Native-Balsa	8±1	245±9	9.3±1.6	7.5±1.3	0.12
Native-Balsa-Clay	8±1	229±12	8.6±0.8	6.8±1.5	0.1
Delignified-Balsa	8±1	296±11	10.8±1.3	5.5±1	*
Delignified-Balsa-Clay	8±1	157±9	7.4±1.2	3±1	*

TTI, time to ignition; pKHRR, peak heat release rate; THR, total heat release; SPR, smoke production rate; TSR, total smoke release. '*' the value is too small to be detected.

The final residues show completely different structures for the samples

with or without clay nanoparticles (Figure 5.16c). Delignified balsa and native balsa without clay nanoparticles result in a TSR around 0.1 m^2 (Table 5.3), the residue appears more compact and less fragile. Clay nanoplatelets improve thermal insulation and mechanical properties of the charred layer. The surface protection layer does not break and combustion kinetics is reduced (Figure 5.16c). Delignified balsa clay sample showed the lowest CO/CO_2 release, smoke production rate (SPR) and total smoke release (TSR) (Table 5.3). After burning, the final residue structure is preserved due to the unique nanostructure of clay nanoplatelets embedded inside the cell wall. This structure is efficient in reducing oxygen permeability and improving thermal stability of the char.[101]

5.4 Highly porous wood/epoxy nanocomposite for liquid separation (Paper V)

5.4.1 Epoxy infiltration into the wood cell wall

A key challenge for functionalization of wood is the accessibility of molecules into the cell wall during impregnation. Epoxies are widely used as thermoset resins for fiber composite.[102–104] It has been suggested that low molecular weight resin easily penetrates into the cell wall. Compatibility between epoxy and wood is another issue for wood modification. Surface modification is one of the strategies for compatibility study. Despite this, the swelling of the cell wall increases the fiber volume so that epoxy resins can diffuse into the cell wall.[105] An idea of the infiltration of epoxy resin into the cell wall is schematically shown in Figure 5.17, nanoporosity in the cell wall is generated after delignification of the native wood structure (Figure 5.17, left). The epoxy resin of bisphenol A diglycidyl ether (DGEBA) and Jeffamine D-400 polyetheramine (PEA) in acetone is then impregnated into the cell wall of the delignified wood template with vacuum infiltration.

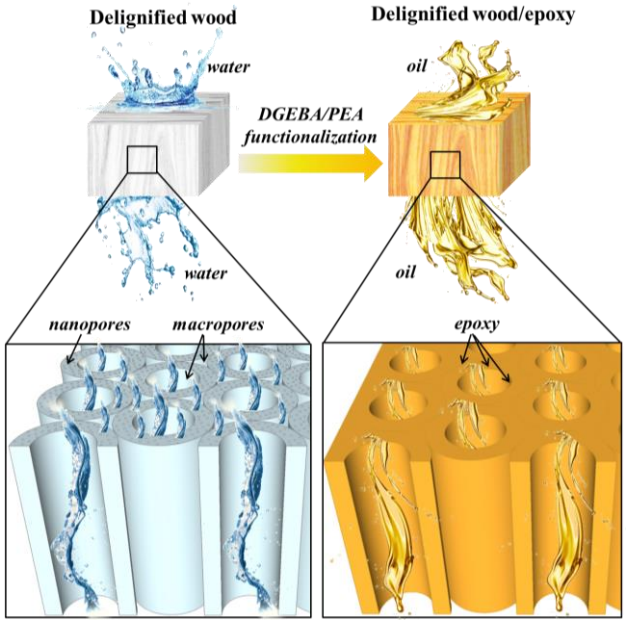

Figure 5.17 Schematic illustration of structural design of highly porous and functional wood materials including the delignified wood template (left) and delignified wood/epoxy biocomposite (right).

5.4.2 Structure of the wood/epoxy biocomposite

High magnification SEM images reveal the epoxy infiltrated in the cell wall (Figure 5.18). The delignified wood template was impregnated with 5 wt% of epoxy/amine acetone solution followed by curing in an oven. After modification with epoxy, the color appears yellow due to infiltration of DGEBA-based epoxy in the microstructure (Figure 5.18a). The epoxy weight content in the delignified balsa wood/epoxy biocomposite is 20.3%. Interestingly, the lumen spaces remain empty (Figure 5.18b) after the evaporation of acetone. The high magnification SEM images show that epoxides were located in the cell wall corner and middle lamella (yellow dash line in Figure 5.18c), as well as inside the cell wall (Figure 5.18d).

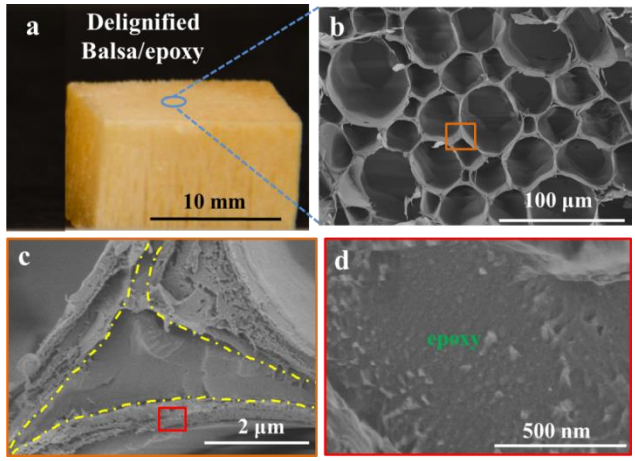

Figure 5.18 The hierarchical structure demonstrated by (a) photograph of the delignified wood/epoxy composite and the cross-sectional FE-SEM images of the cell walls including (b) honeycomb-like cell wall structure at low magnification, (c) the cell walls and (d) secondary cell wall S2 layer at high magnification.

The estimated nanoscale pore volume distribution versus pore size in the range of 2-90 nm for native balsa, delignified balsa and the delignified balsa/epoxy biocomposite are compared in Figure 5.19. Mesoporous size in the range of 2-20 nm is the largest pore volume fraction for the delignified balsa template. Both curves of native balsa and delignified balsa/epoxy biocomposite exhibit similar trend of pore volume distribution. This is also in line with similar porosity (around 88%) for both native balsa and the delignified balsa/epoxy composite. Together with Figure 5.18, it can be concluded that the pores created in the cell wall by delignification are successfully infiltrated with epoxy resin.

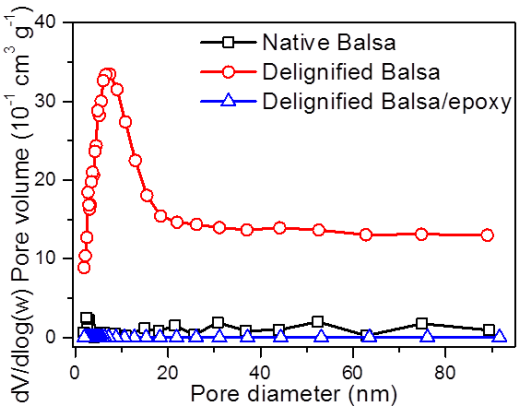

Figure 5.19 Pore volume distributions of balsa wood, delignified balsa and the delignified wood/epoxy biocomposite.

5.4.3 Properties of the wood/epoxy biocomposite

The hydrophobicity of delignified balsa wood template and the delignified wood/epoxy composite was evaluated by using contact angle measurement (Figure 5.20). When a drop of water was placed on the surface in longitudinal direction, the water droplet was immediately absorbed into the samples of native wood and the delignified wood template (Figure 5.20a,b). For the delignified balsa wood/epoxy biocomposite, the initial contact angle was rather high (140°) and decreased slightly to 125° over a period of 3 min (Figure 5.20c). This indicates that the delignified balsa wood/epoxy biocomposite is not only hydrophobic, but also showing much lower rate of water absorption. On the contrary, the highly porous delignified wood template is hydrophilic. The hydrophobicity of the delignified balsa wood/epoxy biocomposite is ascribed to cell wall modification through the impregnation with epoxy. The nano-scale pores inside the cell walls of the delignified wood template were replaced by epoxy (Figure 5.18). The hydroxyl groups of cellulose on the exposed surfaces were also modified covalently by the epoxy resin.[105]

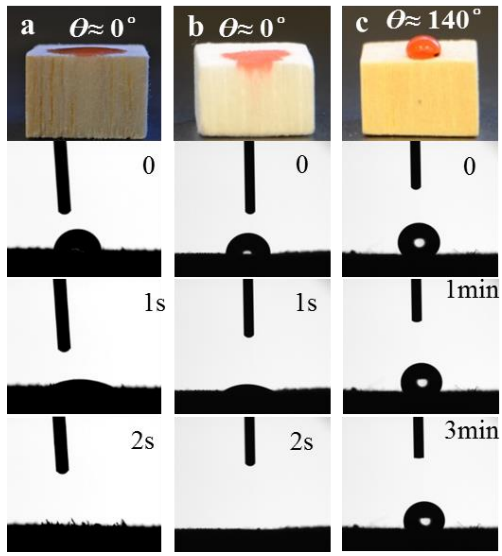

Figure 5.20 Water absorption of balsa, delignified wood template and delignified wood/epoxy biocomposite. Photographs of a water (dyed with Congo Red) droplet on the surface of (a) balsa, (b) delignified wood template and (c) delignified wood/epoxy biocomposite at 0 s, 1 s, 2 s, 1 min, and 3 min.

The selective oil adsorption was demonstrated by touching the droplet of methylene chloride (dyed with Oil Red O) that was spilled out at the bottom of water with native balsa, the delignified balsa wood template and the delignified balsa wood/epoxy biocomposite (Figure 5.21a-c). The oil droplet could not be absorbed because water was instantaneously absorbed into native balsa and the delignified balsa template in 8s (Figure 5.21a,b). Nanoporosity in the cell wall facilitates water absorption due to capillary action and thus improves the hydrophilicity for the delignified wood. In addition, the extraction of hydrophobic lignin leads to exposure of the hydrophilic cellulose microfibrils in the fiber walls. In contrast, the oil droplet was immediately absorbed by the delignified balsa/epoxy composite in 3s (Figure 5.21c). Water absorption capacity was significantly decreased from 28 g/g for the delignified wood template to 0.3 g/g for the delignified balsa wood/epoxy biocomposite (Figure 5.21d). This can be explained by the coating of a thin layer of hydrophobic epoxy polymer between cell wall surfaces. The absorption

capacities of different oils were around 6-15 g/g for the delignified balsa wood/epoxy biocomposite (Figure 5.21e). With these characteristics, the delignified balsa wood template and the delignified balsa wood/epoxy biocomposite could be used for applications in oil/water separation.

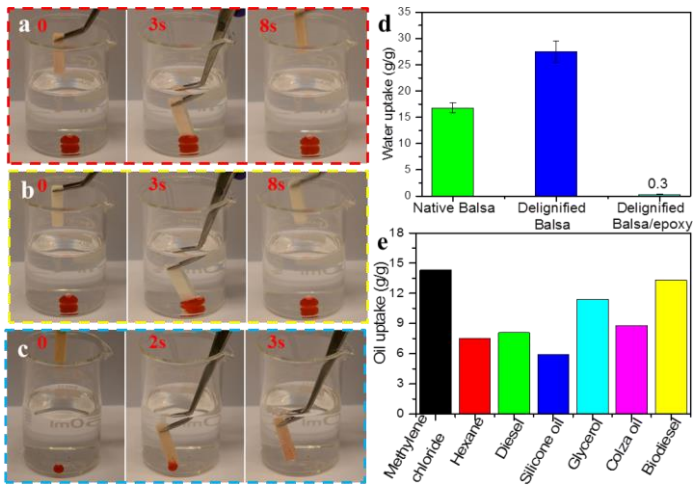

Figure 5.21 Demonstration of underwater adsorption of methylene chloride (dyed with Oil Red O) using (a) native balsa wood; (b) delignified balsa wood template and (c) delignified balsa wood/epoxy biocomposite. (d) Water absorption capacity of the wood structures. (e) Absorption capacities of different oils for delignified wood/epoxy composite.

6. Conclusions

The present thesis investigates the preparation of delignified or bleached wood templates and nanostructural functionalization of wood. Various delignification approaches are carried out, and results for cell wall structures are investigated in terms of the size and distribution of the resulting nano- and microscale porosity, as well as the specific surface area. Removal of lignin results in microscale pores at cell wall corners, more homogeneously distributed nanoscale pores of 2-90 nm and specific surface areas as high as 20-50 m^2/g. These templates offer hierarchical porosity with microscale lumen channels combined with nanoscale cell wall porosity, where the solid material is dominated by nanocellulose fibrils. This is of great interest as a scaffold for biobased materials providing new functionalities. Wood structures were also successfully subjected to bleaching only, for the purpose of preserving mechanical integrity while removing chromophores.

Delignified and nanoporous templates were soaked in hydrocolloidal nanoclay suspensions. This resulted in inorganic hybrid wood structures of improved fire retardancy. It was verified that after treatment, clay nanoparticles were present in the cell wall of delignified templates. This methodology opens a route for nanoparticle modified wood hybrids. Important fire retardancy mechanisms included clay-supported charring of the wood cell wall tissue. In addition, the gas barrier properties of the clay are likely to suppress emission of volatiles as well as oxygen diffusion into the polymeric substances of the cell wall.

Delignified templates were also used to prepare hydrophobic/oleophilic wood/epoxy biocomposites for separation of oil/water mixtures. A procedure was developed where epoxy precursors were successfully impregnated into

the cell wall and cured, and the epoxy location was verified.

Optically transparent wood for engineering purposes was prepared by impregnating wood template pore space with MMA monomer/oligomers. Refractive index of PMMA is similar to cellulose. An optical transmittance of 85% was obtained at 1.2 mm thickness. Cellulose volume fraction was controlled by template compression, which increased mechanical properties but decreased transmittance of the composite. The material was analysed as a composite and synergy effects were revealed, so that the composite showed better properties than both the porous wood template and the PMMA. In order to obtain more isotropic optical and mechanical properties, a plywood approach was developed as a means to tailor composite properties.

Chemical bleaching to remove chromophoric substances can also be used for transparent wood preparation. The advantage is that the mechanical stability of the template is improved compared with delignification approaches. Compared with alternative transparent materials, such as glass, the present material is more ductile with much higher work of fracture.

Wood nanotechnology for nanoscale modification is in its infancy. Transparent wood, fire retardant wood and wood for liquid separation purposes are examples of potential applications of wood modified at molecular and nanostructural scale. Mechanical performance, liquid transport properties and large-scale potential can still be retained as new functionalities are added. This also points to a need for improved characterization methods for nanostructural details in the new types of modified wood presented in the present thesis.

7. Future work

Nanoporous wood templates can be used in new wood nanotechnologies for functional materials. Higher density wood species should be the focus of further investigation, since they provide better mechanical properties but also puts challenges on optical transmittance. Better understanding of the nanopore structure in the cell wall, its chemical nature and mechanisms for monomer diffusion and polymerization are also desirable. From the point of view of optical transmittance, mechanisms for light-material interactions and light propagation need to be investigated. Furthermore, alternative polymers to replace PMMA, which combine matched refractive index with biobased origin need to be explored.

New applications of wood nanotechnology are explored, such as photonics, water purification, and energy storage devices. In any wood functionalization process, the basic properties of wood should be taken advantage of. This includes its biobased origin, comparably low cost, hierarchical structure, mechanical performance, liquid transport function, anisotropy and availability. This will ensure successful applications for large-scale industrial use.

Acknowledgements

First of all, I would like to express my sincere gratitude to Prof. Lars Berglund for useful scientific criticism, discussions, and guidance. He is gratefully acknowledged for the patient supervision that has shaped the thesis. His deep scientific insights and critical feedbacks have been the most important sources of motivation.

I also would like to thank my co-supervisor, Prof. Qi Zhou, for his helpful advice and the discussion on the manuscripts. Dr. Yuanyuan Li is also greatly acknowledged for running the "transparent wood" project together and for the scientific discussions. I am grateful to my co-authors (Federico, Min and Martin L.) for scientific contribution.

The Wallenberg Wood Science Center (WWSC) is gratefully acknowledged for providing lab facilities. I would also like to thank China Scholarship Council for financial support of my PhD study.

I am thankful to current and former colleagues at Biocomposites group, WWSC, and FPT, for the positivity during this "marathon" journey. I would like to appreciate Dr. Min Yan and Dr. Ilya Sychugov for providing optical measurement at Kista. Xuan (Justin), Lilian and Farhan are acknowledged for helpful and scientific discussions during the "coffee time". Ramiro, Thèrése and Pia are thanked for the lab and office related support. Shun, Alireza, Erik, Jakob, Pan, Qiong, Thomas and all other colleagues at WWSC and FPT are thanked for their kindness and making the workplace enjoyable. Yingxin, Valentina and Varvara (Stockholm University) are appreciated for valuable help.

Most importantly, I am forever grateful to my dear family (my parents, Qixian, Qiru and Qimei), who offer endless moral support and boundless love. All of their love, encouragement and support have been instrumental in

putting me where I am. In the end, I would like to specially thank my wife (Xiaolian) for the constant company and motivation she has provided; for moral support; for taking extra duties just so that I could focus on my studies. I am truly grateful for that!

References

1. Tarkow, H.; Stamm, A. J.; others. *Acetylated Wood*; Wis.: US Dept. of Agriculture, Forest Products Laboratory: Madison, **1955**.
2. Hill, C. *Wood Modification: Chemical, Thermal and Other Processes.*; John Wiley & Sons Inc.: Hoboken, **2006**.
3. Harrington, J. J. Hierarchical Modelling of Softwood Hygro-Elastic Properties. *PhD Thesis, Univ. Canterbury*, **2002**.
4. Walker, J. C. F. *Primary Wood Processing: Principles and Practice*; Springer Science & Business Media: Dordrecht, **2006**.
5. Gibson, L. J.; Ashby, M. F. *Cellular Solids: Structure and Properties*; Cambridge University Press: Cambridge, **1999**.
6. Rowell, R. *Handbook of Wood Chemistry and Wood Composites*; CRS Press: Florida, **2005**.
7. Sjöström, E. *Wood Chemistry: Fundamentals and Applications*; Academic Press Inc: California, **1993**.
8. Hill, C. A. S.; Papadopoulos, A. N. A Review of Methods Used to Determine the Size of the Cell Wall Microvoids of Wood. *J. Inst. Wood Sci.* **2001**, *15*, 337–345.
9. Plötze, M.; Niemz, P. Porosity and Pore Size Distribution of Different Wood Types as Determined by Mercury Intrusion Porosimetry. *Eur. J. Wood Wood Prod.* **2011**, *69*, 649–657.
10. Yin, J.; Song, K.; Lu, Y.; Zhao, G.; Yin, Y. Comparison of Changes in Micropores and Mesopores in the Wood Cell Walls of Sapwood and Heartwood. *Wood Sci. Technol.* **2015**, *49*, 987–1001.
11. Borrega, M.; Gibson, L. J. Mechanics of Balsa (Ochroma Pyramidale) Wood. *Mech. Mater.* **2015**, *84*, 75–90.
12. Ermeydan, M. A. Wood Cell Wall Modification With Hydrophobic Molecules. *PhD Thesis, Max Planck Insititute Colloids Interface - Univ.*

Potsdam, **2014**.

13. Sernek, M.; Resnik, J.; Kamke, F. A. Penetration of Liquid Urea-Formaldehyde Adhesive into Beech Wood. *Wood Fiber Sci.* **1999**, *31*, 41–48.

14. Lozhechnikova, A.; Bellanger, H.; Michen, B.; Burgert, I.; Österberg, M. Surfactant-Free Carnauba Wax Dispersion and Its Use for Layer-by-Layer Assembled Protective Surface Coatings on Wood. *Appl. Surf. Sci.* **2017**, *396*, 1273–1281.

15. Burgert, I.; Cabane, E.; Zollfrank, C.; Berglund, L. Bio-Inspired Functional Wood-Based Materials – Hybrids and Replicates. *Int. Mater. Rev.* **2015**, *60*, 431–450.

16. Chen, C.; Zhang, Y.; Li, Y.; Dai, J.; Song, J.; Yao, Y.; Gong, Y.; Kierzewski, I.; Xie, J.; Hu, L. All-Wood, Low Tortuosity, Aqueous, Biodegradable Supercapacitors with Ultra-High Capacitance. *Energy Environ. Sci.* **2017**, *10*, 538–545.

17. Lv, S.; Fu, F.; Wang, S.; Huang, J.; Hu, L. Novel Wood-Based All-Solid-State Flexible Supercapacitors Fabricated with a Natural Porous Wood Slice and Polypyrrole. *RSC Adv.* **2015**, *5*, 2813–2818.

18. Ye, R.; Chyan, Y.; Zhang, J.; Li, Y.; Han, X.; Kittrell, C.; Tour, J. M. Laser-Induced Graphene Formation on Wood. *Adv. Mater.* **2017**, *29*, 1702211.

19. Ek, M.; Gellerstedt, G.; Henriksson, G. *Wood Chemistry and Biotechnology*; Walter de Gruyter: Sweden, **2009**.

20. Kadla, J. F.; Chang, H. The Reactions of Peroxides with Lignin and Lignin Model Compounds. In *American Chemical Society: Washington*; **2001**; pp. 108–129.

21. Pan, B. G. X.; Spencer, L.; Leary, G. J. A Comparative Study on Reactions of Hydrogen Peroxide and Peracetic Acid with Lignin Chromophores. *Holzforschung* **2000**, *54*, 144–152.

22. Kumar, R.; Hu, F.; Hubbell, C. A.; Ragauskas, A. J.; Wyman, C. E. Comparison of Laboratory Delignification Methods, Their Selectivity, and Impacts on Physiochemical Characteristics of Cellulosic Biomass. *Bioresour. Technol.* **2013**, *130*, 372–381.

23. Brogdon, B. N.; Lucia, L. A. New Insights into Lignin Modification during Chlorine Dioxide Bleaching Sequences (IV): The Impact of Modifications in the (EP) and (EOP) Stages on the D 1 Stage. *J. Wood Chem. Technol.* **2005**, *25*, 149–170.

24. Ou, R.; Xie, Y.; Wolcott, M. P.; Sui, S.; Wang, Q. Morphology, Mechanical Properties, and Dimensional Stability of Wood Particle/high Density Polyethylene Composites: Effect of Removal of Wood Cell Wall Composition. *Mater. Des.* **2014**, *58*, 339–345.

25. Albrecht, J. S. An Investigation of the Physical-Chemical Mechanism of Selective Delignification of Wood with Peracetic Acid. *PhD Thesis, Georg. Inst. Technol.* **1971**.

26. Agosin, E.; Blanchette, R. A.; Silva, H.; Lapierre, C.; Cease, K. R.; Ibach, R. E.; Abad, A. R.; Muga, P. Characterization of Palo Podrido, a Natural Process of Delignification in Wood. *Appl. Environ. Microbiol.* **1990**, *56*, 65–74.

27. Gierer, J. Chemistry of Delignification - Part 2: Reactions of Lignins during Bleaching. *Wood Sci. Technol.* **1986**, *20*, 1–33.

28. Deshpande, A. S.; Burgert, I.; Paris, O. Hierarchically Structured Ceramics by High-Precision Nanoparticle Casting of Wood. *Small* **2006**, *2*, 994–998.

29. Ermeydan, M. A.; Cabane, E.; Gierlinger, N.; Koetz, J.; Burgert, I. Improvement of Wood Material Properties via in Situ Polymerization of Styrene into Tosylated Cell Walls. *RSC Adv.* **2014**, *4*, 12981–12988.

30. Burgert, I.; Keplinger, T.; Cabane, E.; Merk, V.; Rüggeberg, M. Chapter 13 - Biomaterial Wood: Wood-Based and Bioinspired Materials. In *Secondary Xylem Biology*; Academic Press: Boston, **2016**; pp. 259–281.

31. Cabane, E.; Keplinger, T.; Künniger, T.; Merk, V.; Burgert, I. Functional Lignocellulosic Materials Prepared by ATRP from a Wood Scaffold. *Sci. Rep.* **2016**, *6*, 31287.

32. Paris, O.; Burgert, I.; Fratzl, P. Biomimetics and Biotemplating of Natural Materials. *MRS Bull.* **2010**, *35*, 219–225.

33. Keplinger, T.; Cabane, E.; Chanana, M.; Hass, P.; Merk, V.; Gierlinger, N.; Burgert, I. A Versatile Strategy for Grafting Polymers to Wood Cell Walls. *Acta Biomater.* **2015**, *11*, 256–263.

34. Ermeydan, M. A.; Cabane, E.; Masic, A.; Koetz, J.; Burgert, I. Flavonoid Insertion into Cell Walls Improves Wood Properties. *ACS Appl. Mater. Interfaces* **2012**, *4*, 5782–5789.

35. Cabane, E.; Keplinger, T.; Merk, V.; Hass, P.; Burgert, I. Renewable and Functional Wood Materials by Grafting Polymerization within Cell Walls. *ChemSusChem* **2014**, *7*, 1020–1025.

36. Furuno, T.; Imamura, Y.; Kajita, H. The Modification of Wood by Treatment with Low Molecular Weight Phenol-Formaldehyde Resin: A Properties Enhancement with Neutralized Phenolic-Resin and Resin Penetration into Wood Cell Walls. *Wood Sci. Technol.* **2004**, *37*, 349–361.

37. Gindl, W.; Gupta, H. S. Cell-Wall Hardness and Young's Modulus of Melamine-Modified Spruce Wood by Nano-Indentation. *Composites, Part A* **2002**, *33*, 1141–1145.

38. Gindl, W.; Zargar-Yaghubi, F.; Wimmer, R. Impregnation of Softwood Cell Walls with Melamine-Formaldehyde Resin. *Bioresour. Technol.* **2003**, *87*, 325–330.

39. Xie, Y.; Krause, A.; Militz, H.; Turkulin, H.; Richter, K.; Mai, C. Effect of Treatments with 1,3-Dimethylol-4,5-Dihydroxy-Ethyleneurea (DMDHEU) on the Tensile Properties of Wood. *Holzforschung* **2007**, *61*, 43–50.

40. Emmerich, L.; Bollmus, S.; Militz, H. Wood Modification with DMDHEU (1.3-Dimethylol-4.5-Dihydroxyethyleneurea) – State of the Art, Recent Research Activities and Future Perspectives. *Wood Mater. Sci. Eng.* **2017**, *0*, 1–16.

41. Donath, S.; Militz, H.; Mai, C. Wood Modification with Alkoxysilanes. *Wood Sci. Technol.* **2004**, *38*, 555–566.

42. Xie, Y.; Fu, Q.; Wang, Q.; Xiao, Z.; Militz, H. Effects of Chemical Modification on the Mechanical Properties of Wood. *Eur. J. Wood Wood Prod.* **2013**, *71*, 401–416.

43. Chang, H.; Tu, K.; Wang, X.; Liu, J. Fabrication of Mechanically Durable Superhydrophobic Wood Surfaces Using Polydimethylsiloxane and Silica Nanoparticles. *RSC Adv.* **2015**, *5*, 30647–30653.

44. Wang, X.; Chai, Y.; Liu, J. Formation of Highly Hydrophobic Wood Surfaces Using Silica Nanoparticles Modified with Long-Chain Alkylsilane. *Holzforschung* **2013**, *67*, 667–672.

45. Merk, V.; Chanana, M.; Keplinger, T.; Gaan, S.; Burgert, I. Hybrid Wood Materials with Improved Fire Retardance by Bio-Inspired Mineralisation on the Nano- and Submicron Level. *Green Chem.* **2015**, *17*, 1423–1428.

46. Merk, V.; Chanana, M.; Gaan, S.; Burgert, I. Mineralization of Wood by Calcium Carbonate Insertion for Improved Flame Retardancy. *Holzforschung* **2016**, *70*, 867.

47. Wang, W.; Zhu, Y.; Cao, J. Morphological, Thermal and Dynamic Mechanical Properties of Cathay Poplar/organoclay Composites Prepared by in Situ Process. *Mater. Des.* **2014**, *59*, 233–240.

48. Darder, M.; Aranda, P.; Ruiz-Hitzky, E. Bionanocomposites: A New Concept of Ecological, Bioinspired, and Functional Hybrid Materials. *Adv. Mater.* **2007**, *19*, 1309–1319.

49. Merk, V.; Chanana, M.; Gierlinger, N.; Hirt, A. M.; Burgert, I. Hybrid Wood Materials with Magnetic Anisotropy Dictated by the Hierarchical Cell Structure. *ACS Appl. Mater. Interfaces* **2014**, *6*, 9760–9767.

50. Shin, Y.; Liu, J.; Chang, J. H.; Nie, Z.; Exarhos, G. J. Hierarchically Ordered Ceramics through Surfactant-Templated Sol-Gel Mineralization of Biological Cellular Structures. *Adv. Mater.* **2001**, *13*, 728–732.

51. Cai, X.; Riedl, B.; Zhang, S. Y.; Wan, H. The Impact of the Nature of Nanofillers on the Performance of Wood Polymer Nanocomposites. *Composites, Part A* **2008**, *39*, 727–737.

52. Munch, E.; Launey, M. E.; Alsem, D. H.; Saiz, E.; Tomsia, A. P.; Ritchie, R. O. Tough, Bio-Inspired Hybrid Materials. *Science.* **2008**,

322, 1516–1520.

53. Zollfrank, C.; Scheibel, T.; Seitz, H.; Travitzky, N. Bioinspired Materials Engineering. In *Ullmann's Encyclopedia of Industrial Chemistry*; Wiley-VCH Verlag GmbH & Co. KGaA: Weinheim, Germany, **2014**; pp. 1–22.

54. Guo, B.; Liu, Y.; Zhang, Q.; Wang, F.; Wang, Q.; Liu, Y.; Li, J.; Yu, H. Efficient Flame-Retardant and Smoke-Suppression Properties of Mg–Al-Layered Double-Hydroxide Nanostructures on Wood Substrate. *ACS Appl. Mater. Interfaces* **2017**, *9*, 23039–23047.

55. Sieber, H.; Hoffmann, C.; Kaindl, A.; Greil, P. Biomorphic Cellular Ceramics. *Adv. Eng. Mater.* **2000**, *2*, 105–109.

56. Zollfrank, C.; Kladny, R.; Sieber, H.; Greil, P. Biomorphous SiOC/C-Ceramic Composites from Chemically Modified Wood Templates. *J. Eur. Ceram. Soc.* **2004**, *24*, 479–487.

57. Qian, J.; Wang, J.; Jin, Z. Preparation of Biomorphic SiC Ceramic by Carbothermal Reduction of Oak Wood Charcoal. *Mater. Sci. Eng. A* **2004**, *371*, 229–235.

58. Shin, Y.; Wang, C.; Exarhos, G. J. Synthesis of SiC Ceramics by the Carbothermal Reduction of Mineralized Wood with Silica. *Adv. Mater.* **2005**, *17*, 73–77.

59. Keplinger, T.; Cabane, E.; Berg, J. K.; Segmehl, J. S.; Bock, P.; Burgert, I. Smart Hierarchical Bio-Based Materials by Formation of Stimuli-Responsive Hydrogels inside the Microporous Structure of Wood. *Adv. Mater. Interfaces* **2016**, *3*, 1–6.

60. Chen, F.; Gong, A. S.; Zhu, M.; Chen, G.; Lacey, S. D.; Jiang, F.; Li, Y.; Wang, Y.; Dai, J.; Yao, Y.; *et al.* Mesoporous, Three-Dimensional Wood Membrane Decorated with Nanoparticles for Highly Efficient Water Treatment. *ACS Nano* **2017**, *11*, 4275–4282.

61. Dong, X.; Zhuo, X.; Wei, J.; Zhang, G.; Li, Y. Wood-Based Nanocomposite Derived by in Situ Formation of Organic-Inorganic Hybrid Polymer within Wood via a Sol-Gel Method. *ACS Appl. Mater. Interfaces* **2017**, *9*, 9070–9078.

62. Kojiro, K.; Miki, T.; Sugimoto, H.; Nakajima, M.; Kanayama, K.

Micropores and Mesopores in the Cell Wall of Dry Wood. *J. Wood Sci.* **2010**, *56*, 107–111.

63. Yano, H.; Hirose, A.; Collins, P. J.; Yazaki, Y. Effects of the Removal of Matrix Substances as a Pretreatment in the Production of High Strength Resin Impregnated Wood Based Materials. *J. Mater. Sci. Lett.* **2001**, *20*, 1125–1126.

64. Yano, H. Potential Strength for Resin-Impregnated Compressed Wood. *J. Mater. Sci. Lett.* **2001**, *20*, 1127–1129.

65. Fink, S. Transparent Wood - A New Approach in the Functional-Study of Wood Structure. *Holzforschung.* **1992**, *46*, 403–408.

66. Li, Y.; Fu, Q.; Yu, S.; Yan, M.; Berglund, L. Optically Transparent Wood from a Nanoporous Cellulosic Template: Combining Functional and Structural Performance. *Biomacromolecules* **2016**, *17*, 1358–1364.

67. Sehaqui, H.; Zhou, Q.; Berglund, L. A. High-Porosity Aerogels of High Specific Surface Area Prepared from Nanofibrillated Cellulose (NFC). *Compos. Sci. Technol.* **2011**, *71*, 1593–1599.

68. Kochumalayil, J. J.; Morimune, S.; Nishino, T.; Ikkala, O.; Walther, A.; Berglund, L. A. Nacre-Mimetic Clay/xyloglucan Bionanocomposites: A Chemical Modification Route for Hygromechanical Performance at High Humidity. *Biomacromolecules* **2013**, *14*, 3842–3849.

69. Ansari, F.; Galland, S.; Johansson, M.; Plummer, C. J. G.; Berglund, L. A. Cellulose Nanofiber Network for Moisture Stable, Strong and Ductile Biocomposites and Increased Epoxy Curing Rate. *Composites, Part A* **2014**, *63*, 35–44.

70. Li, Y.; Yu, S.; Veinot, J. G. C.; Linnros, J.; Berglund, L.; Sychugov, I. Luminescent Transparent Wood. *Adv. Opt. Mater.* **2017**, *5*, 1600834.

71. Tappi, T. 222 Om-02: Acid-Insoluble Lignin in Wood and Pulp. *2002--2003 TAPPI Test Methods,* **2002**.

72. Hull, D.; Clyne, T. W. *An Introduction to Composite Materials*; Cambridge University Press: Cambridge, **1996**.

73. Sehaqui, H.; Zhou, Q.; Ikkala, O.; Berglund, L. A. Strong and Tough Cellulose Nanopaper with High Specific Surface Area and Porosity. *Biomacromolecules* **2011**, *12*, 3638–3644.

74. ASTM, D. Standard Test Method for Haze and Luminous Transmittance of Transparent Plastics. *ASTM Int. ASTM Int. West Conshohoken. PA,* **2000**.

75. Labrador, A.; Cerenius, Y.; Svensson, C.; Theodor, K.; Plivelic, T. The Yellow Mini-Hutch for SAXS Experiments at MAX IV Laboratory. In *Journal of Physics: Conference Series*; **2013**, 425, pp. 72019.

76. Benecke, G.; Wagermaier, W.; Li, C.; Schwartzkopf, M.; Flucke, G.; Hoerth, R.; Zizak, I.; Burghammer, M.; Metwalli, E.; Müller-Buschbaum, P.; *et al.* A Customizable Software for Fast Reduction and Analysis of Large X-Ray Scattering Data Sets: Applications of the New DPDAK Package to Small-Angle X-Ray Scattering and Grazing-Incidence Small-Angle X-Ray Scattering. *J. Appl. Crystallogr.* **2014**, *47*, 1797–1803.

77. Donaldson, L. A.; Radotic, K. Fluorescence Lifetime Imaging of Lignin Autofluorescence in Normal and Compression Wood. *J. Microsc.* **2013**, *251*, 178–187.

78. Korhonen, J. T.; Kettunen, M.; Ras, R. H. A.; Ikkala, O. Hydrophobic Nanocellulose Aerogels as Floating, Sustainable, Reusable, and Recyclable Oil Absorbents. *ACS Appl. Mater. Interfaces* **2011**, *3*, 1813–1816.

79. Fritz-Popovski, G.; Van Opdenbosch, D.; Zollfrank, C.; Aichmayer, B.; Paris, O. Development of the Fibrillar and Microfibrillar Structure during Biomimetic Mineralization of Wood. *Adv. Funct. Mater.* **2013**, *23*, 1265–1272.

80. Fritz-Popovski, G.; Morak, R.; Schöberl, T.; Van Opdenbosch, D.; Zollfrank, C.; Paris, O. Pore Characteristics and Mechanical Properties of Silica Templated by Wood. *Bioinspired, Biomim. Nanobiomaterials* **2014**, *3*, 160–168.

81. Fu, Q.; Medina, L.; Li, Y.; Carosio, F.; Hajian, A.; Berglund, L. A. Nanostructured Wood Hybrids for Fire-Retardancy Prepared by

Clay Impregnation into the Cell Wall. *ACS Appl. Mater. Interfaces* **2017**, *9*, 36154–36163.

82. Henriksson, M.; Berglund, L. A.; Isaksson, P.; Lindström, T.; Nishino, T. Cellulose Nanopaper Structures of High Toughness. *Biomacromolecules* **2008**, *9*, 1579–1585.

83. Galland, S.; Berthold, F.; Prakobna, K.; Berglund, L. A. Holocellulose Nanofibers of High Molar Mass and Small Diameter for High-Strength Nanopaper. *Biomacromolecules* **2015**, *16*, 2427–2435.

84. Müller, U.; Rätzsch, M.; Schwanninger, M.; Steiner, M.; Zöbl, H. Yellowing and IR-Changes of Spruce Wood as Result of UV-Irradiation. *J. Photochem. Photobiol. B Biol.* **2003**, *69*, 97–105.

85. Zhu, M.; Song, J.; Li, T.; Gong, A.; Wang, Y.; Dai, J.; Yao, Y.; Luo, W.; Henderson, D.; Hu, L. Highly Anisotropic, Highly Transparent Wood Composites. *Adv. Mater.* **2016**, *28*, 5181–5187.

86. Gan, W.; Xiao, S.; Gao, L.; Gao, R.; Li, J.; Zhan, X. Luminescent and Transparent Wood Composites Fabricated by Poly(methyl Methacrylate) and γ-Fe 2 O 3 @YVO 4 :Eu 3+ Nanoparticle Impregnation. *ACS Sustain. Chem. Eng.* **2017**, *5*, 3855–3862.

87. Pipon, G.; Chirat, C.; Lachenal, D. Comparative Effect of Ozone, Chlorine Dioxide, and Hydrogen Peroxide on Lignin: Reactions Affecting Pulp Colour in the Final Bleaching Stage. *Holzforschung* **2007**, *61*, 628–633.

88. Gellerstedt, G.; Agnemo, R. The Reactions of Lignin with Alkaline Hydrogen Peroxide. Part III. The Oxidation of Conjugated Carbonyl Structures. *Acta Chem. Scand. B* **1980**, *34*, 275–280.

89. Ramos, E.; Calatrava, S. F.; Jiménez, L. Bleaching with Hydrogen Peroxide. A Review. *Afinidad* **2008**, *65*, 366–373.

90. Li, Y.; Fu, Q.; Rojas, R.; Yan, M.; Lawoko, M.; Berglund, L. Lignin-Retaining Transparent Wood. *ChemSusChem* **2017**, *10*, 3445–3451.

91. Agarwal, B. D.; Broutman, L. J.; Chandrashekhara, K. *Analysis and Performance of Fiber Composites*; John Wiley & Sons Inc.: Hoboken, **2015**.

92. Gao, M.; Sun, C. Y.; Wang, C. X. Thermal Degradation of Wood Treated with Flame Retardants. *J. Therm. Anal. Calorim.* **2006**, *85*, 765–769.

93. Byrne, C. E.; Nagle, D. C. Carbonization of Wood for Advanced Materials Applications. *Carbon.* **1997**, *35*, 259–266.

94. Brebu, M.; Vasile, C. Thermal Degradation of Lignin - a Review. *Cellul. Chem. Technol.* **2010**, *44*, 353–363.

95. Tomak, E. D.; Baysal, E.; Peker, H. The Effect of Some Wood Preservatives on the Thermal Degradation of Scots Pine. *Thermochim. Acta* **2012**, *547*, 76–82.

96. Poletto, M.; Zattera, A. J.; Forte, M. M. C.; Santana, R. M. C. Thermal Decomposition of Wood: Influence of Wood Components and Cellulose Crystallite Size. *Bioresour. Technol.* **2012**, *109*, 148–153.

97. Poletto, M.; Zattera, A. J.; Santana, R. M. C. Thermal Decomposition of Wood: Kinetics and Degradation Mechanisms. *Bioresour. Technol.* **2012**, *126*, 7–12.

98. Tian, C. M.; Guo, H. Z.; Zhang, H. Y.; Xu, J. Z.; Shi, J. R. Study on the Thermal Degradation of Cotton Cellulose Ammonium Phosphate and Its Metal Complexes. *Thermochim. Acta* **1995**, *253*, 243–251.

99. Soares, S.; Camino, G.; Levchik, S. Effect of Metal Carboxylates on the Thermal Decomposition of Cellulose. *Polym. Degrad. Stab.* **1998**, *62*, 25–31.

100. Hedberg, E.; Kristensson, A.; Ohlsson, M.; Johansson, C.; Johansson, P. Å.; Swietlicki, E.; Vesely, V.; Wideqvist, U.; Westerholm, R. Chemical and Physical Characterization of Emissions from Birch Wood Combustion in a Wood Stove. *Atmos. Environ.* **2002**, *36*, 4823–4837.

101. Carosio, F.; Kochumalayil, J.; Cuttica, F.; Camino, G.; Berglund, L. Oriented Clay Nanopaper from Biobased Components - Mechanisms for Superior Fire Protection Properties. *ACS Appl. Mater. Interfaces* **2015**, *7*, 5847–5856.

102. Shimazaki, Y.; Miyazaki, Y.; Takezawa, Y.; Nogi, M.; Abe, K.; Ifuku,

S.; Yano, H. Excellent Thermal Conductivity of Transparent Cellulose Nanofiber/Epoxy Resin Nanocomposites. *Biomacromolecules* **2007**, *8*, 2976–2978.

103. Lu, J.; Askeland, P.; Drzal, L. T. Surface Modification of Microfibrillated Cellulose for Epoxy Composite Applications. *Polymer* **2008**, *49*, 1285–1296.

104. Iwamoto, S.; Nakagaito, A. N.; Yano, H.; Nogi, M. Optically Transparent Composites Reinforced with Plant Fiber-Based Nanofibers. *Appl. Phys. A Mater. Sci. Process.* **2005**, *81*, 1109–1112.

105. Ansari, F.; Sjöstedt, A.; Larsson, P. T.; Berglund, L. A.; Wågberg, L. Hierarchical Wood Cellulose Fiber/epoxy Biocomposites - Materials Design of Fiber Porosity and Nanostructure. *Composites, Part A* **2015**, *74*, 60–68.